

JLab Program Advisory Committee Eleven Proposal Cover Sheet

This document must be received by close of business on Wednesday, December 18, 1996 at:

Jefferson Lab
User Liaison Office, Mail Stop 12 B
12000 Jefferson Avenue
Newport News, VA 23606

(Choose one)

New Proposal Title: *Recoil Polarization in Eta Electroproduction*

Update Experiment Number:

Letter-of-Intent Title:

Contact Person

Name: *James J. Kelly*

Institution: *University of Maryland*

Address: *Dept. of Physics*

Address:

City, State ZIP/Country: *College Park, MD 20742, U.S.A.*

Phone: *301-405-6110*

FAX: *301-314-9525*

E-Mail / Internet: *kelly @ enp.umd.edu*

Experimental Hall: *A*

Days Requested for Approval: *26*

Jefferson Lab Use Only

Receipt Date: _____

PR 96-001

By: _____

[Signature]

HAZARD IDENTIFICATION CHECKLIST

JLab Proposal No.: _____
(For CFBAF/Peer Liaison Office use only.)

Date: 12/18/96

Check all items for which there is an anticipated need.

<p>Cryogenics</p> <p><input checked="" type="checkbox"/> beamline magnets</p> <p><input checked="" type="checkbox"/> analysis magnets</p> <p><input checked="" type="checkbox"/> target</p> <p>type: <u>LH₂</u></p> <p>flow rate: _____</p> <p>capacity: <u>10-15 cm cell</u></p>	<p>Electrical Equipment</p> <p>_____ cryo/electrical devices</p> <p>_____ capacitor banks</p> <p>_____ high voltage</p> <p>_____ exposed equipment</p>	<p>Radioactive/Hazardous Materials</p> <p>List any radioactive or hazardous toxic materials planned for use:</p> <p>_____</p> <p>_____</p> <p>_____</p>
<p>Pressure Vessels</p> <p>_____ inside diameter</p> <p>_____ operating pressure</p> <p>_____ window material</p> <p>_____ window thickness</p>	<p>Flammable Gas or Liquids</p> <p>type: _____</p> <p>flow rate: _____</p> <p>capacity: _____</p> <p>Drift Chambers</p> <p>type: <u>HRS + FPP, Hall A</u></p> <p>flow rate: _____</p> <p>capacity: _____</p>	<p>Other Target Materials</p> <p>_____ Beryllium (Be)</p> <p>_____ Lithium (Li)</p> <p>_____ Mercury (Hg)</p> <p>_____ Lead (Pb)</p> <p>_____ Tungsten (W)</p> <p>_____ Uranium (U)</p> <p>_____ Other (list below)</p> <p>_____</p> <p>_____</p>
<p>Vacuum Vessels</p> <p>_____ inside diameter</p> <p>_____ operating pressure</p> <p>_____ window material</p> <p>_____ window thickness</p>	<p>Radioactive Sources</p> <p>_____ permanent installation</p> <p>_____ temporary use</p> <p>type: _____</p> <p>strength: _____</p>	<p>Large Mech. Structure/System</p> <p>_____ lifting devices</p> <p>_____ motion controllers</p> <p>_____ scaffolding or</p> <p>_____ elevated platforms</p>
<p>Lasers</p> <p>type: _____</p> <p>wattage: _____</p> <p>class: _____</p> <p>Installation:</p> <p>_____ permanent</p> <p>_____ temporary</p> <p>Use:</p> <p>_____ calibration</p> <p>_____ alignment</p>	<p>Hazardous Materials</p> <p>_____ cyanide plating materials</p> <p>_____ scintillation oil (from)</p> <p>_____ PCBs</p> <p>_____ methane</p> <p>_____ TMAE</p> <p>_____ TEA</p> <p>_____ photographic developers</p> <p>_____ other (list below)</p> <p>_____</p> <p>_____</p>	<p>General:</p> <p>Experiment Class:</p> <p><input checked="" type="checkbox"/> Base Equipment</p> <p>_____ Temp. Mod. to Base Equip</p> <p>_____ Permanent Mod. to Base Equipment</p> <p>_____ Major New Apparatus</p> <p>Other: _____</p> <p>_____</p>

LAB RESOURCES REQUIREMENTS LIST

JLab Proposal No.: _____
(For CEBAF User/Johnson Office use only.)

Date: 12/18/96

List below significant resources — both equipment and human — that you are requesting from JLab in support of mounting and executing the proposed experiment. Do not include items that will be routinely supplied to all running experiments, such as the base equipment for the hall and technical support for routine operation, installation, and maintenance.

Major Installations (either your equip. or new equip. requested from JLab)

New Support Structures: _____

Data Acquisition/Reduction

Computing Resources: _____

New Software: _____

Major Equipment

Magnets _____

Power Supplies _____

Targets _____

Detectors _____

Electronics _____

Computer Hardware _____

Other _____

Other

base equipment only,
including: HRS², FPP, LH₂ target

Recoil Polarization in η Electroproduction

J.J. Kelly (spokesperson), E.J. Beise, H. Breuer, C.C. Chang, N.S. Chant,
F. Duncan, A. Lung, P.G. Roos, + *students*
University of Maryland, College Park, MD 20742, U.S.A.

A. Sarty (co-spokesperson), S. Barrow, L. Dennis, P. Dragovitsch,
K. Kemper, S. McAleer, G. Riccardi, + *students*
Florida State University, Tallahassee, FL 32306, U.S.A.

W. Bertozzi (co-spokesperson), K. Fissum, S. Gilad, J. Templon,
J. Zhao, Z. Zhou, + *students*
Massachusetts Institute of Technology, Cambridge, MA 02139, U.S.A.

R. Gilman, C. Glashauser, P. Rutt
Rutgers State University, Piscataway, NJ 08854, U.S.A.

R.W. Lourie
SUNY, Stony Brook, NY 11794, U.S.A.

J.M. Finn, C. Perdrisat
The College of William and Mary, Williamsburg, VA 23185, U.S.A.

K. Aniol, M. Epstein, D. Margaziotis
California State University, Los Angeles, CA 90032, U.S.A.

L.B. Weinstein
Old Dominion University, Norfolk, VA 23529, U.S.A.

P. Markowitz
Florida International University, University Park, FL 33199, U.S.A.

V. Punjabi
Norfolk State University, Norfolk, VA 23504, U.S.A.

A. Afanas'ev, J.P. Chen, S. Nanda, A. Saha
TJNAF, Newport News, VA 23606, U.S.A.

D.S. Dale
University of Kentucky, Lexington, KY 40506, U.S.A.

R.W. Gothe
Universität Bonn, Bonn, Germany

M. Benmerrouche
University of Saskatchewan, Saskatoon, SK S7N 5C6, Canada

N.C. Mukhopadhyay
Rensselaer Polytechnic Institute, Troy, NY 12180, U.S.A.

C. Bennhold
George Washington University, Washington, DC 20052, U.S.A.

Abstract

We propose to measure cross section and recoil polarization angular distributions for η electroproduction at $Q^2 = 0.5 \text{ (GeV/c)}^2$ near the $S_{11}(1535)$ resonance. Measurements will be made on both sides of \mathbf{q} covering the full range of c.m. angle in steps of 30° , allowing the response functions R_{LT} , R_{LT}^N , R_{LT}^L , R_{LT}^S , R_{TT}^L , and R_{TT}^S to be separated with high precision.

These proposed measurements will be complete enough for multipole analysis. The R_{TT}^S response function is shown to provide a relatively model-independent measurement of $|E_{0+}|^2$. The unpolarized transverse response function, R_T , may receive important contributions from the $P_{11}(1440)$ resonance, but those contributions are highly model dependent because neither the electroexcitation form factors nor the ηN branching ratio for that resonance are known well. By contrast, P_{11} resonances do not contribute in first-order to R_{TT}^S and the d-wave and nonresonant contributions are also very small. Furthermore, the d-wave contribution to R_{TT}^S can be separated based upon the angular distribution for its contribution to R_{TT}^L . Once $|E_{0+}|^2$ is known, the P_{11} contribution to R_T can be inferred. The d-wave resonances dominate R_{LT} . Information about the longitudinal couplings for the S_{11} and the nondominant resonances can be obtained from the structure of the LT and LT' response functions.

We will also exploit the symmetry $R_{TT}^L = \pm R_T$ for parallel (antiparallel) kinematics to separate the longitudinal and transverse response functions without using the Rosenbluth method. We expect to be able to measure the ratio $\mathcal{R}_\pm = R_L/R_T$, which is practically unknown for this reaction, to a precision of $\delta\mathcal{R}_\pm \sim 0.02$ by this recoil-polarization technique.

Requirements

Beam energy	: 3.2 GeV
Beam polarization	: $\sim 75\%$
Beam current	: $\leq 75 \mu\text{A}$
Target	: 10 cm LH_2
Luminosity	: $2 \times 10^{38} \text{ cm}^2 \text{ s}^{-1}$
Detectors	: HRS ² + FPP
Beam time	: 624 hours

I. INTRODUCTION

Baryon electroexcitation form factors provide important tests of QCD-inspired models of baryon structure. These quantities can be obtained from meson electroproduction reactions of the type $p(\vec{e}, e' \vec{N})x$, where x represents an undetected meson identified by its missing mass. Examples include π , η , η' , or vector mesons. The use of interference and polarized response functions allows the various resonant and non-resonant multipole amplitudes to be more completely characterized than is possible with cross section measurements alone because the interference between a small amplitude and a large amplitude enhances the relative importance of small amplitudes and permits their extraction from the data. For example, Lourie [1,2] has examined the sensitivity of the $p(\vec{e}, e' \vec{p})\pi^0$ reaction to the structure of the $N \rightarrow P_{33}(1232)$ and $P_{11}(1440)$ transitions using various models of the Delta and Roper resonances. In the delta region these measurements should be sensitive to the deformation of the Δ wave function through the E_{1+} and S_{1+} multipoles and hence to the quark structure of the $N \rightarrow \Delta$ transition. In the Roper region, the presence or absence of longitudinal coupling should distinguish between radial excitation or hybrid baryon models.

The electromagnetic transition form factors for excitation of the $S_{11}(1535)$ resonance are particularly interesting because existing data indicate an unusually hard form factor which decreases rather slowly with Q^2 , a behavior that has not been explained by QCD-inspired models. For example, in Fig. 1 we show a phenomenological analysis of total cross section data for η electroproduction near the $S_{11}(1535)$ and $D_{13}(1520)$ resonances that was performed by Haidan [3,4]. The D_{13} form factor has a typical dipole behavior, whereas the S_{11} falls much more slowly. Several recent calculations of the S_{11} form factors are compared in Fig. 2, which shows that there is considerable spread in both normalization and shape. Although both the relativized constituent quark model of Warns *et al.* [5,6] and the light-cone calculation of Konen and Weber [7] predict stiff form factors, neither reproduces the experimental amplitude. Interestingly, the model of Konen and Weber has recently been improved by Stanley and Weber [8], but now $A_{1/2}(Q^2)$ falls more rapidly and fails to reproduce the shape of the experimental form factor.

Although the dominance of the $S_{11}(1535)$ resonance in the $p(e, e'p)\eta$ reaction simplifies the extraction of the transition form factors, the contributions made to the unpolarized differential cross section by underlying resonances with small branching ratios is not negligible. For example, Knöchlein *et al.* [10] have shown that the $P_{11}(1440)$ Roper resonance can have an appreciable effect upon the angular distribution of the unpolarized transverse response function even though the peak of that resonance is below the η -production threshold. The $D_{13}(1520)$, on the other hand, is expected to dominate R_{LT} . However, neither the transition form factors nor the ηN branching ratios for these resonances are known well. Fortunately, we have found that using recoil polarization there does exist a robust signature of the $S_{11}(1535)$ transition that is relatively free of both resonant and nonresonant backgrounds. This

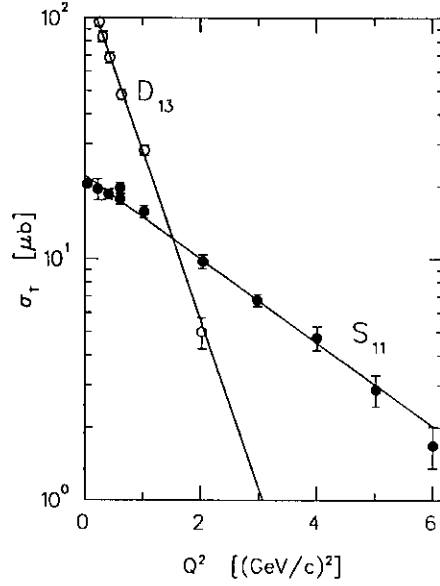


FIG. 1. Total cross section data for electroproduction of the $S_{11}(1535)$ and $D_{13}(1520)$ resonances compiled by Haidan [3,4] show that the S_{11} form factor is unusually stiff.

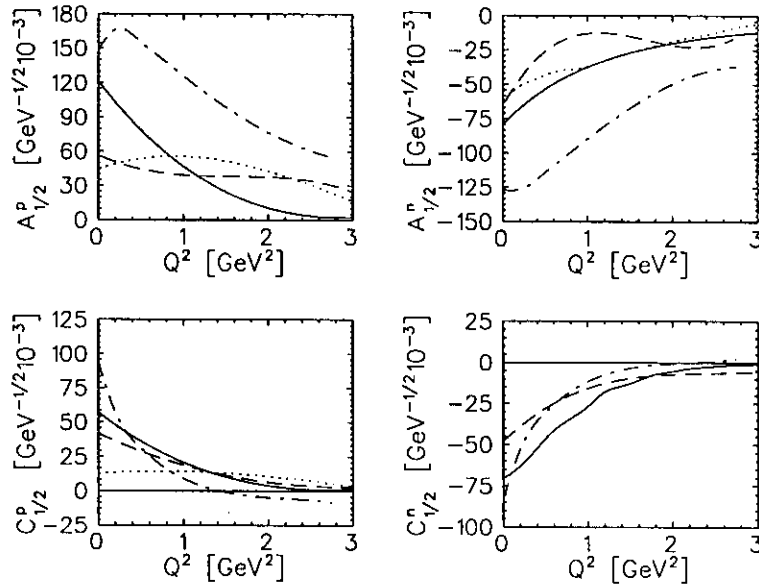


FIG. 2. Electromagnetic helicity amplitudes for excitation of the $S_{11}(1535)$ as predicted by representative quark models. The solid lines are from a nonrelativistic quark model [9,10], dotted lines from a relativized quark model [5,6], dashed lines from a light-cone calculation [7], and dash-dot lines from a light-front calculation [11]. This figure was taken from Ref. [10].

quantity is $R_{TT}^{\prime S}$. Furthermore, a well-chosen set of measurements will also provide considerable information on some of the background resonances as well.

A summary of the data presently available for electromagnetic excitation of the $S_{11}(1535)$ resonance is provided in Table I. High precision photoproduction cross sections have recently been obtained for $W \lesssim 1.51$ GeV by the MAMI-TAPS collaboration, [12], but most of the data for higher W is about 20 years old and of relatively low quality by present standards. Similarly, most of the electroexcitation data is also 20 years old or more and has relatively low precision. Several Rosenbluth separations have been attempted, but the uncertainties in the extracted longitudinal response functions are typically $\pm 50\%$ or more. A couple of low-precision polarization measurements are available for photoproduction [13] and improved experiments are being developed at ELSA, LEGS and GRAAL. No electroexcitation data exists for polarization observables and the sparse data that exists on the azimuthal behavior of the cross section is not adequate for extraction of interference response functions.

TABLE I. Summary of data for η electroproduction. We have not attempted to be truly exhaustive in the citation of older data, but include some representative examples. The quoted kinematic parameters are meant to be descriptive only; for more precise information it is necessary to consult the original references.

target	Q^2 (GeV/c) ²	W GeV	ϵ	θ_η deg.	ϕ_η deg.	measured quantities	lab	date	Ref.
¹ H	0.0	1.487 - 1.493				σ_{tot}	ELSA	1995	[14]
¹ H	0.0	1.485 - 1.537		0 - 180		$d\sigma/d\Omega, \sigma_{tot}$	MAMI	1995	[12]
¹ H	0.0	1.499, 1.514		0 - 180		$d\sigma/d\Omega, \sigma_{tot}$	MIT	1995	[15]
⁴ H	0.0	1.548 - 1.665		45,80,98,112		$d\sigma/d\Omega, \sigma_{tot}$	Tokyo	1988	[16]
¹ H	2.0,3.0	1.5 - 1.8	0.9	0 - 180	0 - 120	$d\sigma/d\Omega, \sigma_{tot}$	DESY	1984	[4]
¹ H	0.6,1.0	1.49 - 1.58	0.5, 0.9	0 - 180	15 - 90	$d\sigma/d\Omega, \sigma_L/\sigma_T$	DESY	1978	[17]
¹ H	0.4	1.44 - 1.64	0.34, 0.79	30 - 140	-40 - 40	$\sigma_{tot}, \sigma_L/\sigma_T$	ELSA	1978	[18]
¹ H	0.22,0.6,1.0	1.505 - 1.715	0.9	60 - 180	0 - 150	$d\sigma/d\Omega, \sigma_{tot}$	DESY	1975	[19]
¹ H	0.2 - 0.4	1.535	0.75	14 - 160	0	$d\sigma/d\Omega, \sigma_{tot}$	ELSA	1974	[20]
¹ H	0.15 - 1.50	1.535		0	0	$d\sigma/d\Omega$	Daresbury	1973	[21]

There are presently two approved η production proposals at TJNAF using the CLAS detector in Hall B. A photoproduction experiment [22] will cover $E_\gamma \leq 2.25$ GeV and an electroproduction experiment [23] will cover $W \leq 1.9$ GeV for $0.2 \leq Q^2 \leq 4.0$ (GeV/c)². These cross section measurements will obtain full angular distributions with high statistics and will extract the unpolarized response functions. However, we shall show that recoil-polarization observables offer some unique sensitivities complementary to those of the unpolarized cross section. Combined analysis of both cross section and polarization data will then markedly improve our ability to disentangle the contributions to this reaction.

We propose to measure recoil polarization in η electroproduction near the $S_{11}(1535)$ resonance for $Q^2 = 0.5$ (GeV/c)². Measurements will be made on both sides of \mathbf{q} so that the helicity-dependent polarizations, P_L' and P_S' , can be separated into LT' and TT' response functions. In particular, one can show that the $R_{TT}^{\prime S}$ response function is strongly dominated by the S_{11} contribution, which can be iso-

lated with very little model uncertainty arising from nonresonant backgrounds or from underlying resonances. By contrast, the unpolarized transverse response function, R_T , can receive an appreciable but highly model-dependent contribution from the poorly understood $P_{11}(1440)$ Roper resonance; the absence of that contribution makes R_{TT}^S the most robust measure of the $N \rightarrow S_{11}(1535)$ electromagnetic transition form factors available. Comparison between R_{TT}^S and R_T can then be used to study the $P_{11}(1440)$ amplitudes. We will also obtain data on the LT response functions dominated by the D_{13} and D_{15} resonances.

In Section II we investigate the sensitivity of recoil polarization observables to various aspects of the eta electroproduction process. In Section III we discuss the experimental procedures for the proposed measurements. In Section IV we summarize our beam time request. A detailed description of our nomenclature for observables and response functions can be found in the appendix.

II. MODELS

We have studied the sensitivity of $p(\vec{e}, e'\vec{p})\eta$ reactions to various aspects of the reaction model using the processes indicated in Fig. 3. The intermediate meson pole was omitted for η electroproduction because the form factor is required by charge-conjugation symmetry to vanish for a self-conjugate meson. The contact diagram indicated in Fig. 3 contributes only for pseudovector (PV) ηNN coupling. Unlike π production for which pseudovector coupling is a consequence of chiral symmetry, there is no fundamental reason to prefer pseudovector (PV) over pseudoscalar (PS) ηNN coupling [24,10,25] and both are available in our code [26]. The analysis of photoproduction data by Tiator *et al.* [24] favored PS coupling with a small coupling constant $g_{\eta NN}^2/4\pi = 0.4$, but Benmerrouche *et al.* [25] find that the existing data can be fitted equally well using a wide range of coupling constants, $0.2 \leq g_{\eta NN} \leq 6.2$. We chose PS coupling for the present calculations because both of those groups have presented parametrizations based upon PS coupling.

Resonant amplitudes for meson electroproduction are often parametrized using an isobar model for the $\gamma_\nu N \rightarrow R \rightarrow \pi N'$ process illustrated in Fig. 4, where for generality we allow π to stand for whatever meson is produced (π , η , η' , etc.). The multipole amplitudes then contain three factors, an electromagnetic transition form factor for the process $\gamma_\nu N \rightarrow R$, a propagator for the intermediate resonance, and a decay amplitude based upon the branching ratio for the process $R \rightarrow \eta N'$, such that [27]

$$A_{t\pm} = \mp C_{\pi N}^I K_{1/2} A_{1/2}^{RN} \quad (1a)$$

$$B_{t\pm} = \pm C_{\pi N}^I K_{3/2} A_{3/2}^{RN} \quad (1b)$$

$$C_{t\pm} = \mp C_{\pi N}^I K_{1/2} C_{1/2}^{RN} = \mp C_{\pi N}^I K_{1/2} \frac{Q}{q^*} S_{1/2}^{RN} \quad (1c)$$

where $C_{\pi N}^I$ is an isospin factor (unity for η production),

$$K_{1/2} = \left[\frac{1}{(2j+1)\pi} \frac{q^* m_N \Gamma_\pi}{p_\pi^* W_R \Gamma^2} \right]^{1/2} \left(\frac{W_R \Gamma}{W^2 - W_R^2 - iW_R \Gamma} \right) \quad (2a)$$

$$K_{3/2} = K_{1/2} \left[\frac{16}{(2j-1)(2j+3)} \right]^{1/2} \quad (2b)$$

are Breit-Wigner factors, and

$$A_{1/2}^{RN} = \sqrt{\frac{2\pi\alpha}{k_\gamma^*}} \xi \langle R, J_z = \frac{1}{2} | J_1^{[1]int} | N, J_z = -\frac{1}{2} \rangle, \quad (3a)$$

$$A_{3/2}^{RN} = \sqrt{\frac{2\pi\alpha}{k_\gamma^*}} \xi \langle R, J_z = \frac{3}{2} | J_1^{[1]int} | N, J_z = \frac{1}{2} \rangle, \quad (3b)$$

$$C_{1/2}^{RN} = \sqrt{\frac{2\pi\alpha}{k_\gamma^*}} \xi \langle R, J_z = \frac{1}{2} | J_0^{[0]int} | N, J_z = \frac{1}{2} \rangle. \quad (3c)$$

are electromagnetic helicity amplitudes for $\gamma_\nu N \rightarrow R$ that are proportional to matrix elements of the electromagnetic current. By convention [9,6], the constant of proportionality includes k_γ^* , which is the c.m. momentum of the virtual photon, and ξ , which is the sign of the $R \rightarrow N'\pi$ decay amplitude (where again π refers to the meson of interest).

To study the sensitivity of various observables to the transition form factors, we employ two models. Knöchlein, Drechsel, and Tiator, hereafter referred to as KDT [10], use a coupled-channels isobar model to analyze π and η production simultaneously. Alternatively, Benmerrouche, Mukhopadhyay, and Zhang, hereafter referred to as BMZ [25], have formulated an effective Lagrangian model for spin-1/2 and spin-3/2 resonances with which the helicity amplitudes can be related directly to form factors associated with the γNR vertex functions. The KDT model provides a more unified treatment of the hadronic decays, whereas the BMZ model provides a more consistent treatment of the electromagnetic vertex. For example, an important difference between these models is that isobar excitation can be found in both the s -channel and the u -channel for BMZ but only in the s -channel for KDT. The s -channel diagram resonates at the isobar mass, m_R , whereas the u -channel diagram is nonresonant for electroproduction kinematics and hence contributes to the nonresonant background. For example, the S_{11} contributes nonresonant M_{1-} and S_{1-} amplitudes in addition to the more familiar resonant E_{0+} and S_{0+} amplitudes.

Both models describe the Born and vector-meson terms using effective Lagrangians of the form

$$\mathcal{L}_{\gamma\eta V} = \frac{g_{\gamma\eta V}}{m_\eta} \varepsilon_{\mu\nu\rho\sigma} \partial^\mu A^\nu \partial^\rho V^\sigma \eta \quad (4a)$$

$$\mathcal{L}_{VNN} = -\bar{N} \left(g_{V1} \gamma_\mu + \frac{g_{V2}}{2m_N} \sigma_{\mu\nu} \partial^\mu V^\nu \right) N \quad (4b)$$

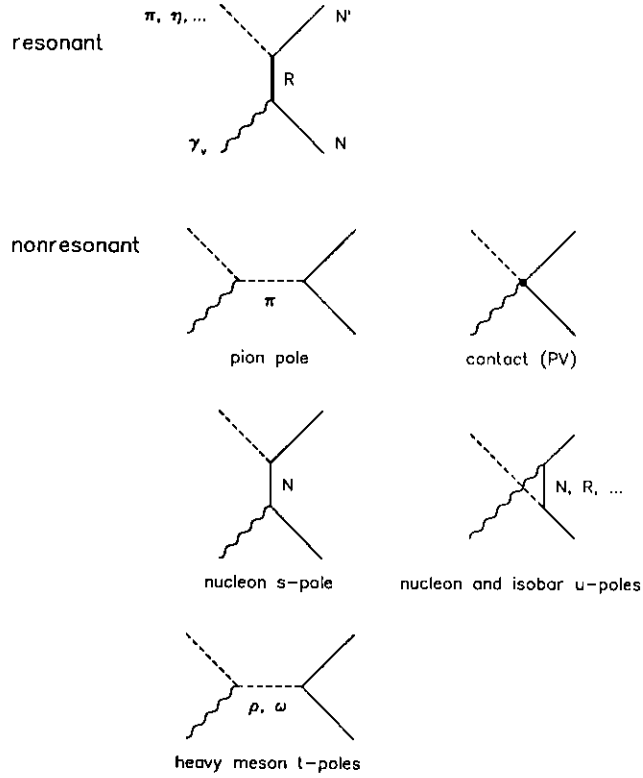


FIG. 3. Selected Feynman diagrams for meson production by a virtual photon. The t -channel pole is included only for charged meson production. The contact diagram is used only for pseudovector coupling.

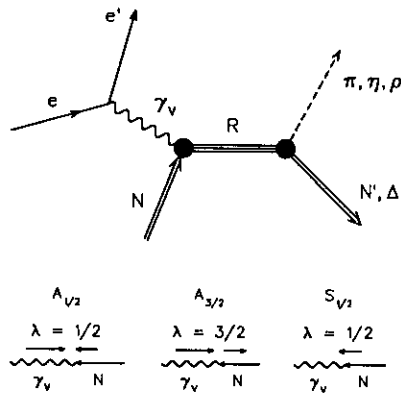


FIG. 4. Isobar model for resonant $\gamma_v N \rightarrow R \rightarrow \eta N'$ amplitudes.

where A^μ is the electromagnetic vector potential, V^σ represents a vector meson, η represents the η -meson field, and N represents a nucleon spinor. A strong form factor,

$$F_{VNN}(t) = \frac{\Lambda_{VNN}^2 - m_V^2}{\Lambda_{VNN}^2 - t} \quad (5)$$

is applied to the VNN vertex according to the prescription of Brown *et al.* [28], and electromagnetic form factors

$$g_{\gamma\eta V}(Q^2) = \frac{e\lambda_{\gamma\eta V}}{1 + \frac{Q^2}{m_V^2}} \quad (6)$$

are applied to the $\gamma\eta V$ vertices. The KDT model includes both ρ and ω , whereas the BMZ use a simpler isospin average.

A. KDT Model

Some of the properties of the η electroproduction reaction are summarized in Table II, which presents the isobar parameters used by KDT [10].

The KDT model does not provide the Q^2 dependence of the electroexcitation form factors directly, but depends upon quark-model predictions. In the calculations which follow, we have employed dipole form factors

$$A_{1/2}, A_{3/2}, C_{1/2} \propto \left(1 + \frac{Q^2}{\Lambda^2}\right)^{-2}$$

with $\Lambda = 1.0$ (GeV/c)² for all γNR form factors. Although undoubtedly simplistic, we can nonetheless explore the possible roles of the P_{11} and D_{13} resonances, for which a complete description is not yet available in the effective lagrangian approach, using the amplitudes in Table II.

The energy-dependent total width for resonance R is parametrized by

$$\Gamma^R(W) = \Gamma^R(W_R) \left[1 + \sum_{f=1}^n b_f^R \left(\frac{\rho_f(W)}{\rho_f(W_R)} - 1 \right) \right] \quad (7)$$

where the summation extends over $f = 1, n$ two-body decay channels with branching ratios

$$b_f^R = \frac{\Gamma_f^R(W_R)}{\Gamma^R(W_R)} \quad (8)$$

TABLE II. Isobar parameters used in the KDT model. The symbol ε represents an isoscalar two-pion-state with mass and width of 800 MeV for the parametrization of uncorrelated two-pion production.

	$S_{11}(1535)$	$P_{11}(1440)$	$D_{13}(1520)$	$D_{15}(1675)$
m_R [MeV]	1544.0	1462.0	1524.0	1676.0
Γ [MeV]	166.0	391.0	124.0	179.0
$A_{1/2}^p$ [10^{-3} GeV $^{-1/2}$]	107	-72	-22	19
$A_{1/2}^n$ [10^{-3} GeV $^{-1/2}$]	-96	52	-62	-47
$A_{3/2}^p$ [10^{-3} GeV $^{-1/2}$]	-	-	163	19
$A_{3/2}^n$ [10^{-3} GeV $^{-1/2}$]	-	-	-137	-69
$C_{1/2}^p$ [10^{-3} GeV $^{-1/2}$]	58	-52	-93	0
$C_{1/2}^n$ [10^{-3} GeV $^{-1/2}$]	-72	0	99	0
meson production multipoles	E_{0+}, L_{0+}	M_{1-}, L_{1-}	E_{2-}, M_{2-}, L_{2-}	E_{2+}, M_{2+}, L_{2+}
electromagnetic multipoles	$E1, C1$	$M1, C0$	$E1, M2, C1$	$E3, M2, C3$
$ f\rangle$	$b_f(m_R)$	$b_f(m_R)$	$b_f(m_R)$	$b_f(m_R)$
ηN	0.50	subthreshold	0.001	0.01
πN	0.40	0.69	0.59	0.47
εN	0.10	0.09	-	-
$(\pi\Delta)_S$	-	-	0.05	-
$(\pi\Delta)_P$	-	0.22	-	-
$(\pi\Delta)_D$	-	-	0.15	0.52
$(\rho_3 N)_D$	-	-	0.21	-

based upon the partial widths at resonance. An energy-independent contribution representing all three-body and more complicated final-states is also included. The phase-space factors

$$\rho_f(W) = \frac{k_f(W)}{W} B_{\ell_f}^2(k_f(W)R_f) \quad (9)$$

are based upon the c.m. relative momentum $k_f(W)$ for invariant mass W and barrier-penetration factors represented by Blatt-Weisskopf functions using interaction radii R_f , taken to be $R_f = 1.0$ fm for all channels. The subthreshold $P_{11}(1440)$ branching ratio was taken from the parametrization of Bennhold and Tanabe [29].

B. BMZ Model

The effective Lagrangian model of Benmerrouche, Mukhopadhyay, and Zhang (BMZ) provides lagrangians $\mathcal{L}_{\gamma NR}$ which describe the excitation of resonance R by a virtual photon at the electromagnetic vertices, $\gamma_\nu N \rightarrow R$. Of greatest interest to the present proposal, using pseudoscalar ηNN coupling the S_{11} resonance is excited by a lagrangian of the form

$$\mathcal{L}_{\gamma NR} = \mathcal{L}_{\gamma NR}^{(1)} + \mathcal{L}_{\gamma NR}^{(2)} \quad (10a)$$

$$\mathcal{L}_{\gamma NR}^{(1)} = \frac{e}{2(M_R + M_N)} \bar{R} \left(G_1^s(Q^2) + G_1^v(Q^2)\tau_3 \right) \gamma_5 \sigma_{\mu\nu} N F^{\mu\nu} + h.c. \quad (10b)$$

$$\mathcal{L}_{\gamma NR}^{(2)} = \frac{e}{(M_R + M_N)^2} \bar{R} \left(G_2^s(Q^2) + G_2^v(Q^2)\tau_3 \right) \gamma_5 \gamma_\mu N \partial_\nu F^{\mu\nu} + h.c. \quad (10c)$$

where N and R indicate nucleon and isobar spinors, G_1^s and G_1^v are isoscalar and isovector Pauli form factors, G_2^s and G_2^v are isoscalar and isovector Dirac form factors, and τ_3 is the target isospin. For pseudovector ηNN coupling there is an additional contact term. Thus, the electromagnetic structure of the $\gamma_\nu p \rightarrow S_{11}$ transition is described by two form factors, $G_1^p(Q^2)$ and $G_2^p(Q^2)$, which are related to the helicity amplitudes by

$$G_1 = \beta(m_R - m_N) \left[\sqrt{2} A_{1/2} - 2 \frac{Q^2}{k_R(m_R - m_N)} C_{1/2} \right] \quad (11a)$$

$$G_2 = \beta(m_R + m_N) \left[\sqrt{2} A_{1/2} + 2 \frac{(m_R - m_N)}{k_R} C_{1/2} \right] \quad (11b)$$

where

$$e\beta = \frac{m_R + m_N}{Q^2 + (m_R - m_N)^2} \left[\frac{m_N(m_R^2 - m_N^2)}{Q_R^+} \right]^{1/2} \quad (12a)$$

$$Q_R^\pm = (m_R \pm m_N)^2 + Q^2 \quad (12b)$$

$$k_R^2 = \frac{Q_R^+ Q_R^-}{4m_R^2} . \quad (12c)$$

BMZ [30] analyzed the existing η electroproduction data and extracted $A_{1/2}(Q^2)$ for the $S_{11}(1535)$ resonance. The results of this analysis are shown in Fig. 5, where the error bars indicate the precision of the experimental data and the band illustrates the sensitivity of the fit to various assumptions about the ratio, $S_{1/2}/A_{1/2}$, between the longitudinal and transverse form factors. To minimize uncertainties due to the branching ratio, it is the quantity

$$\xi_T = \sqrt{\frac{m_N q^*(W_R)}{W_R k^*(W_R)} \Gamma_\eta A_{1/2}(Q^2) / \Gamma} \quad (13)$$

that is actually plotted. The analysis included the nonresonant background (Born terms plus t -channel vector meson exchange) and the S_{11} diagrams for both the resonant s -channel and the nonresonant u -channel, but did not include any resonant backgrounds arising from isobar excitations with small ηN branching ratios. Although the existing data are not sensitive to $S_{1/2}/A_{1/2}$ or to nondominant resonances, it is clear that $A_{1/2}(Q^2)$ is quite stiff. Also shown are predictions based upon a nonrelativistic quark model [31] and a light-front approach [8], neither of which can reproduce the stiffness of the fitted S_{11} electroexcitation form factor. However, the KDT model suggests that the $P_{11}(1440)$ contribution may not be negligible [10].

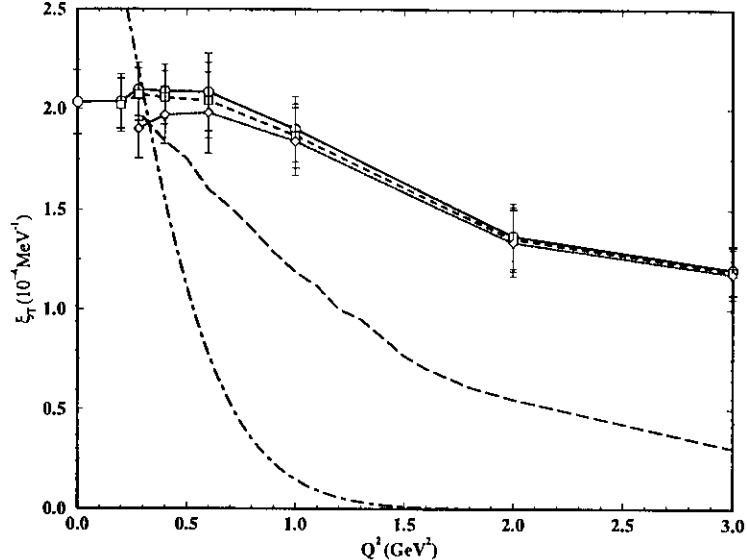


FIG. 5. Fit to $A_{1/2}$ for $S_{11}(1535)$ made by Benmerrouche *et al.* [30]. The quantity ξ_T is shown for several assumptions: circles connected by a solid line use $S_{1/2} = 0$; squares connected by a dashed line use $S_{1/2}/A_{1/2}$ from quark shell model [31]; diamonds connected by a dotted line use $S_{1/2}$ light-front approach of Ref. [8]. The nonrelativistic quark model [31] is shown as a dashed-line and the light-front prediction by a long-dashed line [8].

C. Model Sensitivities

It is instructive to examine the relative importance of various resonant and non-resonant contributions to the total electroproduction cross section, separated into longitudinal and transverse parts. In Fig. 6 we show σ_L and σ_T at $W = 1.535$ GeV and $Q^2 = 0.1$ (GeV/c) 2 for the KDT model. Although the $S_{11}(1535)$ contribution is dominant at the peak, the nonresonant background increases with W . For large W , the destructive interference between these contributions to σ_T significantly reduces the apparent width of the peak and shifts its position slightly. The p-wave and d-wave resonances appear to have negligible effect upon σ_T . The KDT model for σ_L suggests a significant resonant contribution that is much larger than predicted by most quark models, but which is actually scaled to reproduce a single low-precision datum [18] and, hence, cannot be considered reliable. The ratios σ_L/σ_T calculated with the KDT and BMZ models are compared with the limited data in Fig. 7.

In Fig. 8 we compare integrated transverse and longitudinal cross sections calculated with the BMZ and KDT models as functions of photon virtuality. The BMZ model uses the parametrization of $A_{1/2}(Q^2)$ found in Ref. [32], which is very similar to the fit shown in Fig. 5. The KDT model was evaluated using dipole form factors with $\Lambda = 1.0$ GeV/c for all contributing multipoles, but S_{11} is dominant of course. In the BMZ model the transverse cross section falls much more slowly than a typical dipole form factor, but the longitudinal cross section is quite small. In the KDT model, on the other hand, an appreciable longitudinal cross section is

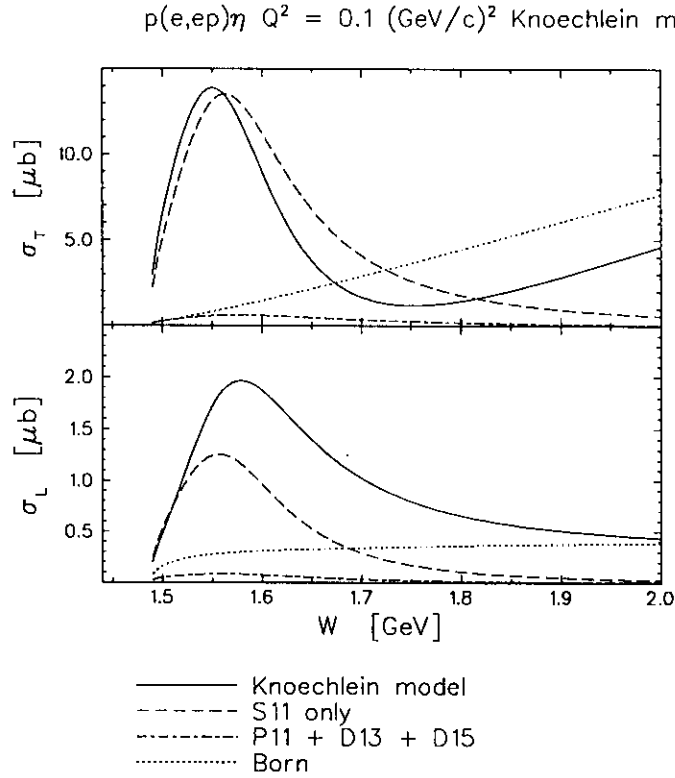


FIG. 6. Resonant and nonresonant contributions to total electroproduction cross sections for $W = 1.535$ GeV and $Q^2 = 0.1$ (GeV/c) 2 using the KDT model. The curves labeled Born include vector-meson exchange.

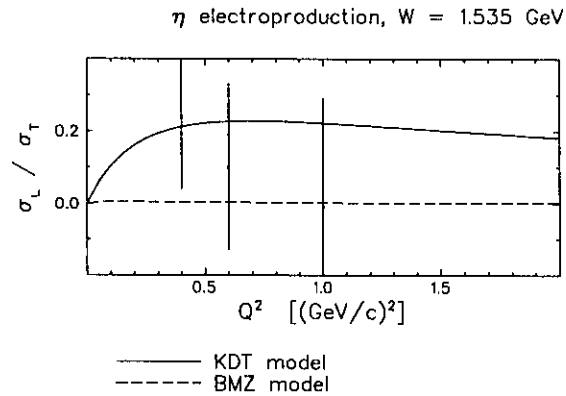


FIG. 7. Ratio between longitudinal and transverse contributions to the total eta production cross section for $W = 1.535$ GeV. The data are from Refs. [18,17].

predicted which, if correct, could require modification of the BMZ fit.

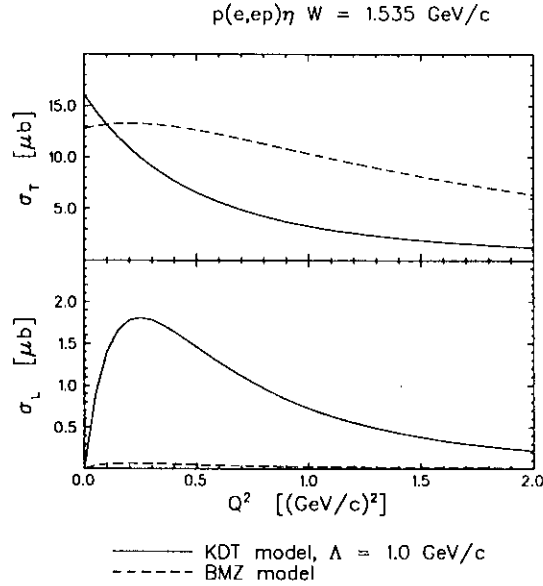


FIG. 8. Integrated transverse and longitudinal cross sections are compared for the BMZ and KDT models. The KDT model is evaluated using dipole form factors with $\Lambda = 1.0$ GeV/c.

If R_L is as large as KDT suggest, it will be possible to obtain a measurement in parallel kinematics by exploiting the symmetry $R_{TT}^L = \pm R_T$ (see Appendix C) to determine the transverse response function for subtraction from the unpolarized differential cross section. The R_{TT}^L response function will be obtained from the recoil polarization measurements and obviates the need for Rosenbluth separation and for careful acceptance matching. We believe that this be the first time that this technique, which is described in more detail in Sec. III A 3, will have been used. Even though the model calculations suggest that there are many small but comparable contributions to R_L that will make it difficult to isolate $C_{1/2}$ for the S_{11} , it should be possible to discriminate between models which give significant longitudinal response functions and those which do not.

A similar decomposition of the coplanar response functions is presented in Fig. 9. One notices that even though the $P_{11}(1440)$ contribution to σ_T appeared negligible, its effect upon the angular distribution for R_T can be quite important. A 10% amplitude which by itself contributes only a 1% partial cross section can nevertheless through interference change the differential cross section by as much as 20%. However, because neither its transition form factor nor its decay branching ratios are known very well, there is considerable uncertainty in that contribution. On the other hand, because $D_{13}(1520)$ has little effect upon R_T or R_{TT}^L , one can separate the $P_{11}(1440)$ and $S_{11}(1535)$ contributions by analyzing those angular distributions. Similarly, the $D_{13}(1520)$ resonance also makes a very small contribution to the integrated cross section but dominates the R_{LT} and R_{TT} interference response functions.

In Fig. 10 we compare calculations and data for $p(e, e'p)\eta$ for $W = 1.535$ GeV at $Q^2 = 0.4$ (GeV/c)². These data [20] were included in the fit made by BMZ to $A_{1/2}(Q^2)$. The KDT model using simple dipole factors with $\Lambda = 1.0$ GeV/c needs to be scaled by a factor of about 1.6 to reproduce these data. The data appear to be consistent with an isotropic angular distribution, but with error bars $\sim \pm 20\%$ the data do not strongly disfavor the deviations from isotropy produced primarily by the $P_{11}(1440)$ contribution to the KDT model either. We propose to obtain cross section angular distributions with statistical uncertainties better than 1% and systematic uncertainties better than 5%.

Coplanar observables predicted by these models for $Q^2 = 0.5$ (GeV/c)² are compared in Fig. 11. The difference between average cross sections is due mostly to the choices of form factor, but the difference in shape reflects the contributions of nondominant resonances included in the KDT model and absent from the BMZ model. The form factors tend to divide out in the polarization observables. The substantial difference in the predictions for P_N is difficult to trace to a single important source because many aspects of the models contribute at similar levels. For the helicity-dependent recoil polarization components the effects of various nondominant resonances can be disentangled by multipole analysis of separated response functions. The roles of these nondominant resonances are illustrated for the KDT model in Fig. 12.

Examination of Fig. 9 suggests that the response function that is most strongly dominated by the $S_{11}(1535)$ resonance is R'_{TT}^S , for which removal of nonresonant backgrounds and/or nondominant resonances appears to have very little effect. This apparent insensitivity to contributions other than S_{11} can be understood by examining the multipole decompositions presented in Appendix B. Those decompositions were derived by Knöchlein *et al.* [10] assuming dominance of the S_{11} resonance. Examining the multipole expansion of R'_{TT}^S , one finds that to first order there are no M_{1-} contributions. Although d-wave resonances enter through interference with the E_{0+} multipole, their contribution remains relatively small. Furthermore, the d-wave contribution can be distinguished and removed based upon its contribution to the angular distribution for R'_{TT}^L . Thus, for R'_{TT}^S one finds that the model-dependent and poorly known P_{11} and D_{13} contributions are strongly suppressed; nor does the nonresonant background contribute significantly to R'_{TT}^S . Therefore, R'_{TT}^S provides a relatively model-independent signal for $|E_{0+}|^2$.

In Fig. 13 we compare coplanar response functions calculated using the BMZ and KDT models. The R'_{TT}^S response functions have similar shapes but differ in scale because $A_{1/2}(Q^2)$ falls less rapidly for BMZ than for the dipole form factor used with the KDT model. Similarly, most of the T -type and TT -type response functions are larger for the BMZ model because $A_{1/2}$ for S_{11} is larger. However, it is also important to recognize that there are shape differences arising primarily from background contributions; for example, R_T is closer to isotropic because the present implementation of the BMZ model lacks a P_{11} term. Conversely, most of the L -type and LT -type response functions are much smaller for the BMZ model

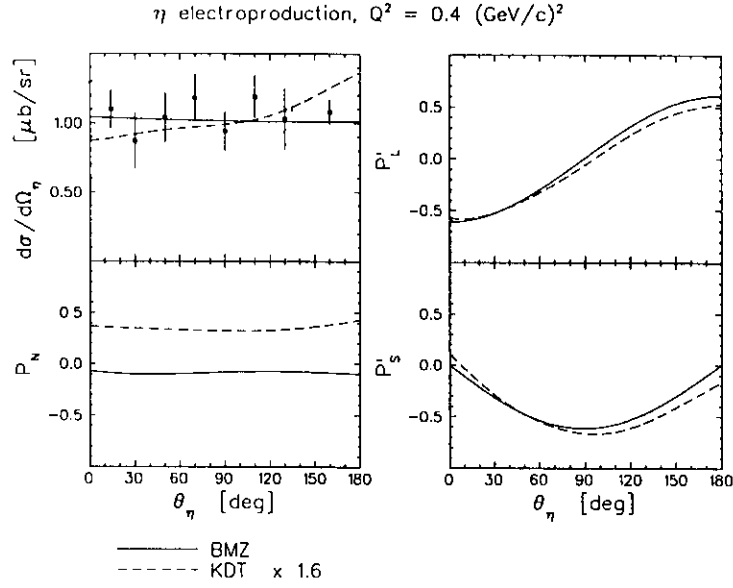


FIG. 10. Comparison between KDT and BMZ models with cross section data for $W = 1.535 \text{ GeV}$ and $Q^2 = 0.4 \text{ (GeV/c)}^2$. The data from [20] were obtained with $\epsilon = 0.79$. The KDT model was scaled by a factor of 1.6. Polarization predictions are compared also.

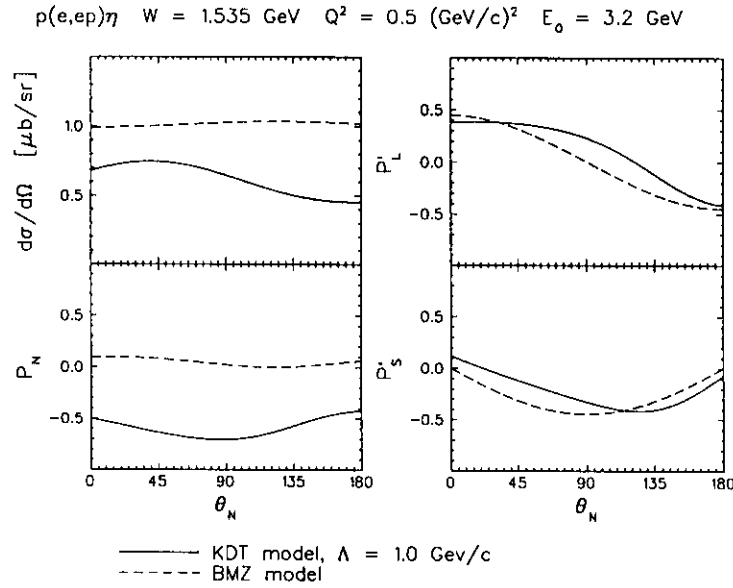


FIG. 11. Comparison between BMZ and KDT models of coplanar observables for $Q^2 = 0.5 \text{ (GeV/c)}^2$.

$p(e,ep)\eta$ $W = 1.535$ GeV $Q^2 = 0.5$ (GeV/c) 2 $E_0 = 3.2$ GeV

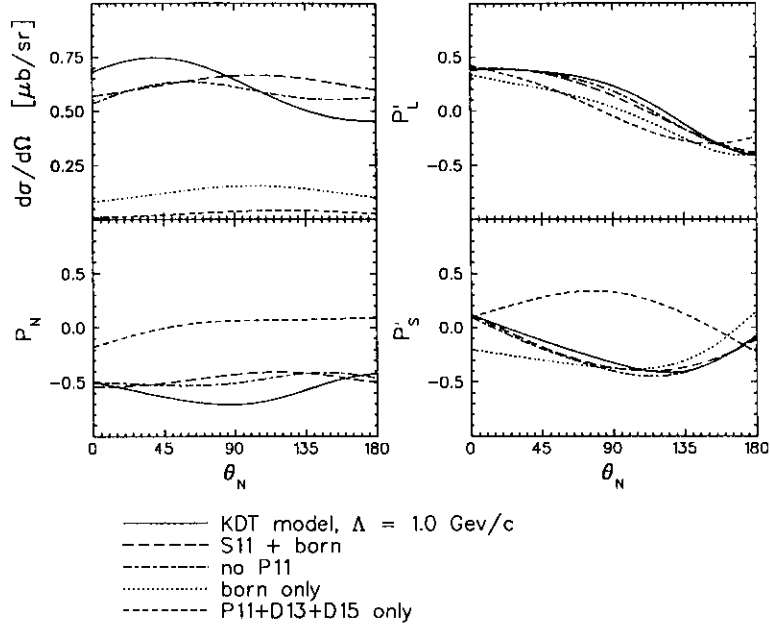


FIG. 12. Various contributions to the KDT model of coplanar observables for $Q^2 = 0.5$ (GeV/c) 2 are shown. The curves labeled Born include vector-meson exchange.

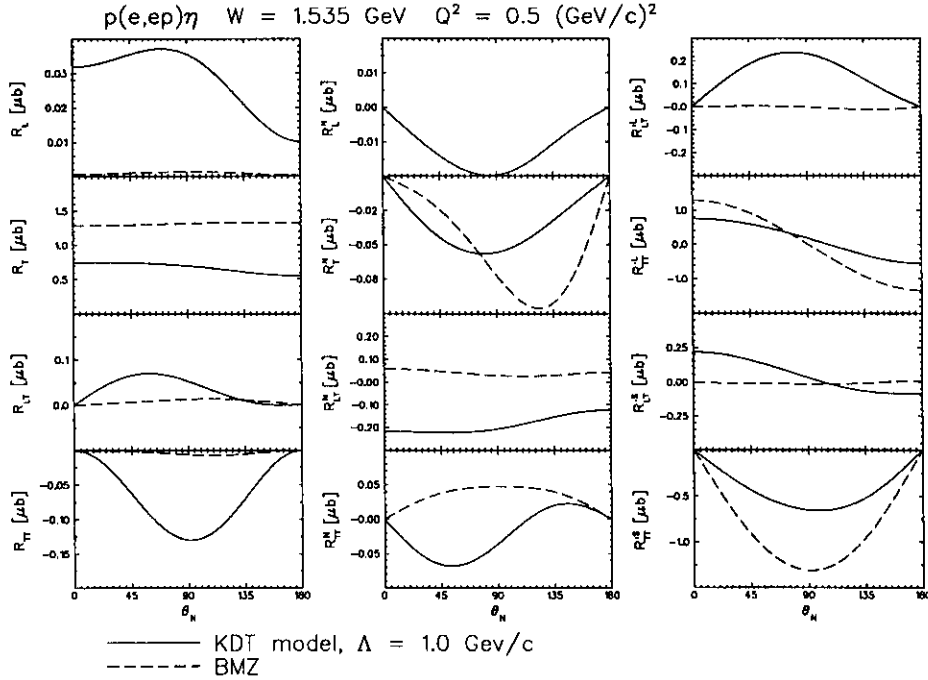


FIG. 13. Comparison between KDT and BMZ models of coplanar response functions for $W = 1.535$ GeV and $Q^2 = 0.5$ (GeV/c) 2 .

III. EXPERIMENTAL PROCEDURE

A. Proposed Measurements

We propose to measure angular distributions for $W = 1.535$ GeV and $Q^2 = 0.5$ (GeV/c)² in coplanar kinematics, obtaining both cross sections and recoil polarization using polarized beam. Adequate coverage of the angular distribution can be obtained using 30° steps in the center of mass angle, θ_N^* . The proposed kinematics are summarized in Table III. We have chosen Q^2 large enough to distinguish between models of the transition form factors without reducing the cross section too much. These kinematics also permit the entire angular distribution to be obtained on both sides of \mathbf{q} without bringing the proton spectrometer prohibitively close to the beam. For $E_0 = 3.2$ GeV the relatively large values of ν_L and ν_{LT} will enhance the sensitivity to the longitudinal and longitudinal-transverse response functions.

For the purposes of making beam time estimates, we discuss in the next few subsections the statistical uncertainties in recoil-polarization measurements and the propagation of those uncertainties through the extraction of response functions. Of course, the analysis of experimental data must also include systematic uncertainties in beam polarization, polarimeter analyzing power and alignment, and kinematic factors. For the helicity-dependent response functions, the systematic uncertainties in beam polarization and analyzing power are expected to total 5 – 8%. For the P_N measurements we expect that it should be possible to keep false asymmetries below 0.01 based upon the experience with the MIT-Bates focal-plane polarimeter [33]. Those contributions will increase the uncertainties somewhat, but do not directly affect beam time requirements. The systematic errors for recoil polarization measurements in Hall A will be investigated, and hopefully minimized, by the upcoming commissioning experiments.

1. Recoil Polarization Measurements

By Fourier analysis of the azimuthal distribution for FPP events, two independent components can be extracted each with a statistical accuracy of

$$\delta\Pi = \frac{\pi}{2\overline{A}_y} \sqrt{\frac{1}{fN}} \quad (14)$$

where \overline{A}_y is the mean analyzing power, f is the fraction of the total number of spectrometer events, N , which are scattered by the analyzer and are accepted for polarization analysis. For coplanar kinematics the net polarization, Π , produced by the reaction can be expressed as

$$\Pi = P_y \hat{y} + h [P'_x \hat{x} + P'_z \hat{z}] \quad (15)$$

TABLE III. Proposed Kinematics

$W = 1.535 \text{ GeV}$	$Q^2 = 0.5 \text{ (GeV/c)}^2$	$\nu_L = 4.421$
$\varepsilon_i = 3.20 \text{ GeV}$	$\varepsilon_f = 2.15 \text{ GeV}$	$\nu_{LT} = 4.092$
$\theta_e = 15.5^\circ$	$\theta_q = 26.9^\circ$	$\nu_{TT} = 0.893$
$\Gamma_\gamma = 3.66 \times 10^{-3} \text{ (GeV sr)}^{-1}$	$\epsilon = 0.893$	$\nu'_{LT} = 0.971$
		$\nu'_{TT} = 0.449$

θ_N^* deg	θ_{pq} deg	p_N GeV/c	$\frac{d\Omega^*}{d\Omega}$
0	0.0	1.029	31.2
± 30	± 5.28	1.001	32.1
± 60	± 9.94	0.923	36.7
± 90	± 13.12	0.811	66.0
± 120	± 13.37	0.689	61.9
± 150	± 8.97	0.590	13.6
180	0.0	0.551	9.0

where \hat{z} is along the nucleon momentum, \hat{x} is in the reaction plane and transverse to the momentum, and \hat{y} is normal to the reaction plane. The polarization measured in the focal plane, Π^{fp} , is then

$$\Pi_x = \Pi_2^{fp} \quad (16a)$$

$$\Pi_y = \Pi_1^{fp} \cos \chi - \Pi_3^{fp} \sin \chi \quad (16b)$$

$$\Pi_z = \Pi_1^{fp} \sin \chi + \Pi_3^{fp} \cos \chi \quad (16c)$$

where Π_1^{fp} is in the dispersion direction, Π_2^{fp} is normal to the bend plane, Π_3^{fp} is along the trajectory, and

$$\chi = \frac{g-2}{2} \gamma \Omega_B \quad (17)$$

is the angle through the proton spin precesses for a bending angle Ω_B . Although Π_3^{fp} cannot be measured by the FPP, the fact that Π_z changes sign with the beam helicity whereas Π_y does not allows separation of the focal-plane polarization within the spectrometer bend plane into two independent reaction components using

$$P_y = \frac{\Pi_1^{fp}(+h) + \Pi_1^{fp}(-h)}{2 \cos \chi} \quad (18a)$$

$$P'_z = \frac{\Pi_1^{fp}(+h) - \Pi_1^{fp}(-h)}{2h \sin \chi} \quad (18b)$$

Therefore, the statistical uncertainties in the recoil polarization components become

$$\delta P'_x = \frac{\delta \Pi}{h}, \quad \delta P_y = \frac{\delta \Pi}{\cos \chi}, \quad \delta P'_z = \frac{\delta \Pi}{h \sin \chi} \quad (19)$$

2. Interference Response Functions

The symmetry with respect to \mathbf{q} is used to separate R_{LT} , R_{LT}^N , R_{LT}^S , R_{TT}^S , R_{LT}^L , and R_{TT}^L for nonparallel kinematics according to

$$R_{LT}(\theta) = [\tilde{\sigma}_0(\theta) - \tilde{\sigma}_0(-\theta)] / 2\nu_{LT} \quad (20a)$$

$$R_{LT}^N(\theta) = [\tilde{\sigma}_y(\theta) + \tilde{\sigma}_y(-\theta)] / 2\nu_{LT} \quad (20b)$$

$$R_{LT}^S(\theta) = [\tilde{\sigma}_x(\theta) + \tilde{\sigma}_x(-\theta)] / 2\nu'_{LT} \quad (20c)$$

$$R_{TT}^S(\theta) = [\tilde{\sigma}_x(\theta) - \tilde{\sigma}_x(-\theta)] / 2\nu'_{TT} \quad (20d)$$

$$R_{LT}^L(\theta) = [\tilde{\sigma}_z(\theta) - \tilde{\sigma}_z(-\theta)] / 2\nu'_{LT} \quad (20e)$$

$$R_{TT}^L(\theta) = [\tilde{\sigma}_z(\theta) + \tilde{\sigma}_z(-\theta)] / 2\nu'_{TT} \quad (20f)$$

where $\tilde{\sigma}_x = \tilde{\sigma}_0 P'_x$, $\tilde{\sigma}_y = \tilde{\sigma}_0 P_y$, and $\tilde{\sigma}_z = \tilde{\sigma}_0 P'_z$ and where positive (negative) angles refer to the left (right) side of \mathbf{q} for electron scattering to the left. In addition, the combinations $\nu_L R_L + \nu_T R_T + \nu_{TT} R_{TT}$ and $\nu_L R_L^N + \nu_T R_T^N + \nu_{TT} R_{TT}^N$ will be obtained but cannot be decomposed further. Thus, assuming that the statistical uncertainty in cross section is negligible, we can separate polarized response functions with statistical uncertainties

$$\delta R_{LT}^N = \frac{\sqrt{2} \delta \Pi}{\nu_{LT} \cos \chi} \tilde{\sigma}_0 \quad (21a)$$

$$\delta R_{LT}^L = \frac{\sqrt{2} \delta \Pi}{h\nu'_{LT} \sin \chi} \tilde{\sigma}_0 \quad \delta R_{TT}^L = \frac{\sqrt{2} \delta \Pi}{h\nu'_{TT} \sin \chi} \tilde{\sigma}_0 \quad (21b)$$

$$\delta R_{LT}^S = \frac{\sqrt{2} \delta \Pi}{h\nu'_{LT}} \tilde{\sigma}_0 \quad \delta R_{TT}^S = \frac{\sqrt{2} \delta \Pi}{h\nu'_{TT}} \tilde{\sigma}_0 \quad (21c)$$

For parallel or antiparallel kinematics each of the polarization measurements can be related directly to an interference response function. Hence, again assuming that the statistical uncertainty in the cross section is negligible, the uncertainties in these response functions become

$$\delta R_{LT}^N = \frac{\delta \Pi}{\nu_{LT} \cos \chi} \tilde{\sigma}_0 \quad (22a)$$

$$\delta R_{TT}^L = \frac{\delta \Pi}{h\nu'_{TT} \sin \chi} \tilde{\sigma}_0 \quad (22b)$$

$$\delta R_{LT}^S = \frac{\delta \Pi}{h\nu'_{LT}} \tilde{\sigma}_0 \quad (22c)$$

The statistical uncertainties in polarization response functions based upon proposed goals for $\delta \Pi$ and the expected performance of the polarimeter are listed in Table IV. Actual experimental uncertainties will be slightly larger due to systematic

uncertainties in beam polarization and polarimeter analyzing power. Nevertheless, these uncertainties will be sufficient to distinguish between various models of this reaction and to perform multipole analysis.

The uncertainty in R_{LT}^N becomes fairly large for $\theta_N^* \rightarrow 180^\circ$ because χ becomes unfavorable. In addition, the normal component may be affected by false asymmetries within the polarimeter and by uncertainties in spin precession, particularly when $\cos \chi \rightarrow 0$. Although measurements of R_{LT}^N for $\theta_N^* \rightarrow 180^\circ$ could be made more easily at larger Q^2 , we have not attempted to optimize the kinematics to improve the measurement of P_N because the physics content of R_{LT}^N is rather model dependent, which is typical of response functions generated by the imaginary part of interference products. We are much more interested in the induced polarization, for which $\sin \chi \sim 1$ is optimal; data for the normal component of polarization will come for free but is not the primary goal of this experiment.

TABLE IV. Projected statistical uncertainties in polarization response functions based upon a statistical accuracy $\delta\Pi$ in each component of the focal-plane polarization and assuming $h = 0.75$.

θ_N^* deg	p_N GeV/c	χ deg	$\delta\Pi$	δR_{TT}^S μb	δR_{LT}^S μb	δR_{TT}^L μb	δR_{LT}^L μb	δR_{LT}^N μb
0	1.029	119.7	0.01		0.013	0.034		0.0050
± 30	1.001	118.6	0.01	0.042	0.019	0.048	0.022	0.0072
± 60	0.923	113.2	0.01	0.042	0.019	0.046	0.021	0.0088
± 90	0.811	106.7	0.01	0.042	0.019	0.044	0.020	0.012
± 120	0.689	100.1	0.01	0.042	0.019	0.043	0.020	0.020
± 150	0.590	95.3	0.02	0.084	0.039	0.084	0.039	0.075
180	0.551	93.5	0.02		0.028	0.059		0.078

3. Longitudinal and Transverse Response Functions

The measurement in parallel kinematics uses the symmetry property

$$\text{parallel kinematics} \implies R_T = \pm R_{TT}^L \quad (23a)$$

$$R_L = [\tilde{\sigma}_0 \mp \nu_T R_T] / \nu_L = \frac{\tilde{\sigma}_0}{\nu_L} \left[1 \mp \frac{\nu_T}{h\nu_{TT}'} \Pi_L \right], \quad (23b)$$

where the upper (lower) sign refers to parallel (antiparallel) kinematics, to separate the longitudinal and transverse response functions without using the Rosenbluth procedure. Since this symmetry does not appear to be commonly known, even though it is not a new result, we provide a derivation and discussion in Appendix C. The recoil-polarization method avoids the careful matching of phase-space acceptances that is needed for Rosenbluth separation based upon two or more rather

different electron scattering kinematics. The uncertainty, δR_L , in the longitudinal response function due to the two uncorrelated uncertainties $\delta\tilde{\sigma}_0$ and $\delta\Pi_L$ is then obtained from the quadrature formula

$$(\delta R_L)^2 = \left(R_L \frac{\delta\tilde{\sigma}_0}{\tilde{\sigma}_0} \right)^2 + \left(\frac{\nu_T}{h\nu'_{TT}\nu_L} \tilde{\sigma}_0 \delta\Pi_L \right)^2 \quad (24)$$

where we assume that the uncertainties in beam polarization and kinematic factors are negligible. Furthermore, if we assume that the relative uncertainty in the cross section is much less than the uncertainty in a polarization measurement, we expect to obtain the longitudinal response function with an uncertainty of about

$$\delta R_L \approx \frac{\nu_T}{\nu_L} \delta R'_{TT} \quad (25)$$

For our kinematics, this uncertainty is $\delta R_L \approx 0.01 \mu\text{b}$ when the uncertainty in polarization measurements is $\delta\Pi_L = 0.015$. This precision is sufficient to discern the longitudinal response predicted by the KDT model, for example, and is competitive with the Rosenbluth technique (e.g. CEBAF proposal PR 94-119).

It is also of interest to examine the ratio between the longitudinal and transverse response functions, which in this approach becomes

$$\mathcal{R}_\pm = \frac{R_L}{R_T} = \frac{\pm h\nu'_{TT} - \nu_T \Pi_L}{\nu_L \Pi_L}. \quad (26)$$

Thus, assuming that the uncertainties in the beam polarization and kinematic factors are negligible, the uncertainty in \mathcal{R}_\pm becomes

$$\delta\mathcal{R}_\pm = \frac{h\nu'_{TT}}{\nu_L \Pi_L^2} \delta\Pi_L = \frac{(\nu_T + \nu_L \mathcal{R}_\pm)^2}{h\nu_L \nu'_{TT}} \delta\Pi_L. \quad (27)$$

Unlike Rosenbluth separation, which requires two independent cross section measurements with rather different electron scattering kinematics and different phase-space acceptances, this procedure yields a ratio that is independent of the normalization of the cross section and does not require moving spectrometers or changing beam energy. Furthermore, as shown by the beam time estimates below, the measurements require substantially less beam time than traditional Rosenbluth separations. Therefore, this technique offers an attractive alternative to Rosenbluth separation with better control over systematic errors. For our kinematics, a recoil-polarization measurement with precision $\delta\Pi_L = 0.015$ would give $\delta\mathcal{R}_\pm \approx 0.02$ if $\mathcal{R}_\pm \approx 0.1$. Depending upon the outcome of this experiment, we anticipate a subsequent proposal to measure the longitudinal form factor for parallel kinematics over a substantial range of Q^2 .

B. Count Rate Estimates

Count rate estimates were made based upon the parameters summarized in Table V. We require a liquid hydrogen target and luminosities up to about $2 \times 10^{38} \text{ cm}^{-2}\text{s}^{-1}$, which corresponds to about $75 \mu\text{A}$ on a 10 cm cell. These conditions require a cooling power of about 250 W, which is well within the design goal for the Hall A cryogenic target. A similar target has been tested in Hall C and shown to operate with less than 1% density fluctuations at a power of approximately 450 W [34]. We also assume a beam polarization of 0.75 based upon the anticipated performance of high-power mode-locked lasers under development at TJNAF for use with high-polarization strained GaAs crystals. If these goals for the polarized source are not realized, compromises on current and/or polarization can be made without losing more than a factor of two in statistical precision or seriously jeopardizing the physics objectives of the experiment.

TABLE V. Count Rate Assumptions

target, power	LH2, 250 W
luminosity	$L \sim 2 \times 10^8 (\mu\text{b s})^{-1}$
solid angles	$\Delta\Omega_e \approx \Delta\Omega_p \approx 6 \text{ msr}$
W bin	$W = 1.535 \pm 0.010 \text{ GeV}$
beam polarization	$h \sim 0.75$
isotropic unpolarized cross section	$\bar{\sigma}_0 \approx 1 \mu\text{b/sr}$

A Monte Carlo code [35] was used to estimate counting rates for finite acceptances and to evaluate resolutions in missing mass, invariant energy, and scattering angle. The beam energy was assumed to have a spread $\sigma(E_0)/E_0 = 5 \times 10^{-5}$ and both spectrometers were assumed to have momentum resolutions $\delta p/p = 10^{-4}$ FWHM. Angular resolutions within and transverse to the bend plane of $\delta\theta_V = 0.59 \text{ mr}$ and $\delta\theta_H = 1.18 \text{ mr}$ were used for the electron spectrometer. For the proton spectrometer, $\delta\theta_V = 1.0 \text{ mr}$ and $\delta\theta_H = 2.35 \text{ mr}$ include multiple scattering in the detectors. Multiple scattering in the target, windows, and air gaps was included also. The resolution in invariant mass of approximately 1.4 MeV FWHM is determined solely by the electron scattering kinematics. The resolution in missing mass is found to vary between 1.0 MeV for parallel kinematics and 3.0 MeV FWHM for $(\theta_N^*, \phi_N) \approx (90^\circ, 0^\circ)$. The resolution in θ_N^* is typically about 1° or better.

The acceptances in θ_N^* versus W are illustrated in Fig. 14, where the twelve independent spectrometer settings covering the full angular range are labeled sequentially and are clearly distinct. The acceptance in invariant mass is smallest for $(\theta_N^*, \phi_N) \approx (90^\circ, 0^\circ)$, but remains large enough to capture a bin of width $\pm 10 \text{ MeV}$. The counting rates listed in Table VI were calculated for the central bin of invariant energy, $W = 1.535 \pm 0.010 \text{ GeV}$, assuming that each spectrometer will have a useful solid angle of 6 msr and momentum acceptance of $\pm 5\%$.

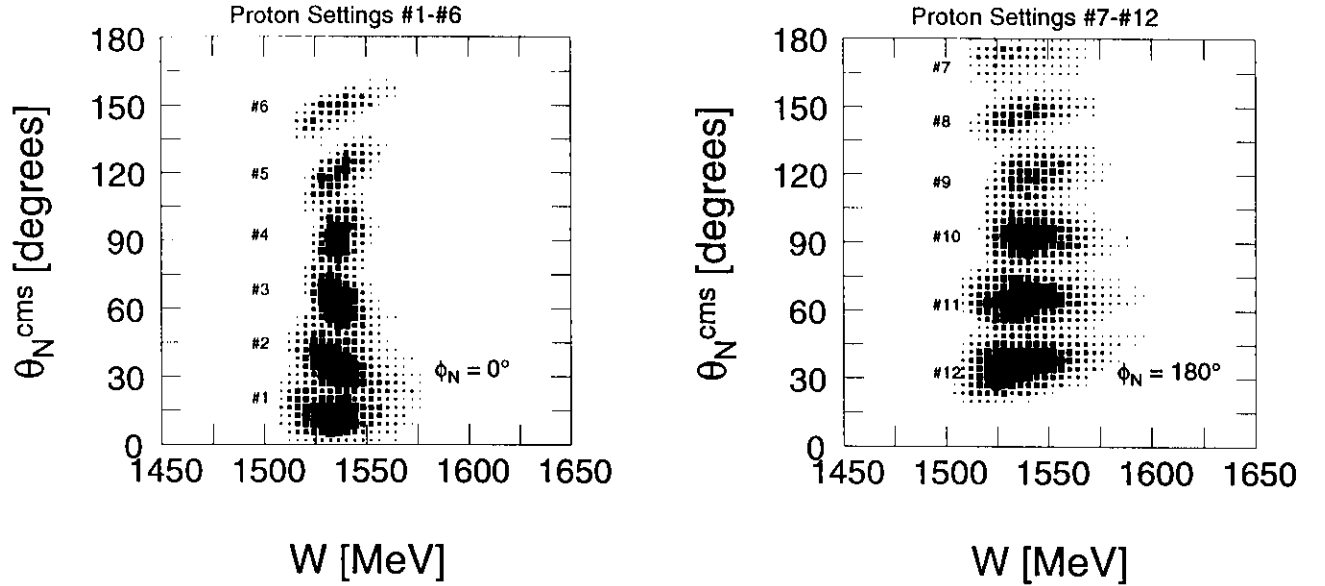


FIG. 14. Simulated acceptances in θ_N^* versus W .

In Fig. 15 we show a simulation of the missing mass spectrum for the central bin of invariant mass produced for the kinematics that are expected to have the least favorable signal/noise ratio. The simulation includes both accidental ($e, e'p$) events and real $p(e, e')\pi\pi$ background events. Singles rates were estimated using modified versions of the Lightbody and O'Connell codes, QFS and EPC [36] and the accidental-coincidence rates were based upon a coincidence timing bin of 1.0 ns. The $p(e, e')\pi\pi$ events were generated with a phase-space distribution normalized to the background rates observed in earlier ($e, e'p$) experiments with similar kinematics [18] assuming that accidental coincidences were negligible for their much smaller luminosities. With a pion rejection rate near 10^{-6} , the $(e, e'\pi^+)$ background should be negligible. Signal-to-noise ratios, S/N , were estimated for 20 MeV bins of invariant energy. These estimated singles rates, background rates, and the signal/noise ratios are presented in Table VII. This ratio is expected to be better than 8:1 for all settings proposed.

For small θ_N^* we find that the multipion background dominates, but for large θ_N^* the accidental coincidences become the most important. Nevertheless, the signal/noise ratio, $S/N \geq 8$, remains quite acceptable even for the least favorable circumstances, which are depicted in Fig. 15. Although the focal-plane detectors were designed to handle rates of 1 MHz with less than 1% dead time, the π^+ rates on the small-angle side of \mathbf{q} may require the luminosity to be reduced and beam time increased for several of those settings. Fortunately, those adjustments are not expected to be large and more accurate estimates will soon be available from commissioning studies for the Hall A spectrometers.

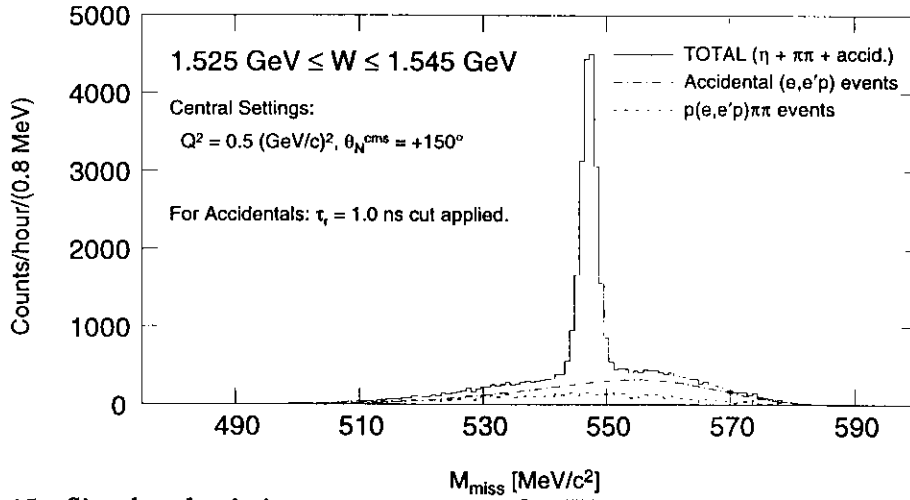


FIG. 15. Simulated missing mass spectrum for $W = 1.535 \pm 0.010$ GeV, $Q^2 = 0.5$ (GeV/c) 2 , and $\theta_N^* = 150^\circ$ including both accidental ($e, e'p$) and real $p(e, e'p)\pi\pi$ background events.

TABLE VI. Count Rate Estimates. The total number of counts required at each setting is designated N . For the purposes of estimating the beam time requirements, the counting rate \bar{R} is averaged for $\phi = 0, \pi$. The time column includes a factor of 2 for nonparallel kinematics requiring two settings.

θ_N^* deg	θ_{pq} deg	p_N GeV/c	\bar{R} s^{-1}	f	\bar{A}_y	$\delta\Pi$	$10^{-6}N$	time hr
0	0.0	1.029	22	0.076	0.36	0.01	2.50	36
± 30	± 5.28	1.001	22	0.076	0.38	0.01	2.25	64
± 60	± 9.94	0.923	22	0.074	0.44	0.01	1.72	48
± 90	± 13.12	0.811	18	0.072	0.51	0.01	1.32	48
± 120	± 13.37	0.689	11	0.066	0.52	0.01	1.38	80
± 150	± 8.97	0.590	7	0.033	0.43	0.02	1.01	96
180	0.0	0.551	4	0.030	0.39	0.02	1.35	192

TABLE VII. Singles and Accidental Coincidence Rates. The accidental $(e, e'p)$ rate assumes a coincidence resolving time of $\tau_{res} = 1.0$ ns and requires $W = 1.535 \pm 0.010$ GeV and $M_{miss} = 0.5475 \pm 0.0025$ GeV.

θ_N^* deg	(e, e') kHz	(e, π^-) kHz	(e, p) kHz	(e, π^+) kHz	accidentals kHz	$(e, e'p)\pi\pi$ kHz	$(e, e'p)\eta$ Hz	S/N
0	129	32	124	192	0.25	1.0	22.1	18
+30			177	381	0.39	1.0	23.2	17
+60			236	731	0.63	1.1	22.9	13
+90			273	1137	0.83	0.82	18.3	11
+120			264	1323	0.72	0.47	10.4	9
+150			220	1148	0.49	0.29	6.2	8
180			173	761	0.38	0.19	4.6	8
-150			141	413	0.39	0.35	7.8	11
-120			111	208	0.44	0.58	11.5	11
-90			88	120	0.32	0.76	18.0	17
-60			81	95	0.22	0.88	21.0	19
-30			92	114	0.19	0.90	21.8	20

C. Sensitivity of Proposed Measurements

The sensitivity of the proposed measurements is illustrated in Figs. 16 and 17 which show the proposed measurements and corresponding response functions with projected statistical uncertainties. The solid curves are based upon the BMZ model and the dashed curves on the KDT model scaled by a factor of 1.6 to obtain approximately the same average cross section as represented by R_T for parallel kinematics. Although such simple scaling is not entirely fair to either model, it does serve to indicate the discriminatory power of the proposed measurements. For example, the R_{TT}^S response functions have slightly different magnitudes even after scaling because the scale factor is sensitive to the P_{11} contribution to R_T in the KDT model which is absent for R_{TT}^S . However, the small difference between the shapes of R_{TT}^S for these models arises primarily from the nonresonant background whose strength relative to the S_{11} contribution is overestimated by the simple scaling applied to the KDT model. The longitudinal couplings for both the S_{11} and the nondominant resonances in the KDT model give the LT and LT' response functions a richer structure which should be readily apparent in the proposed data set. This data set will be complete enough to permit nearly model-independent extraction of the most important multipole amplitudes.

Additional systematic errors of 5 – 8% in the response functions will not affect the discriminatory power of the proposed measurements. Furthermore, Lourie *et al.* [37] have shown for pion electroproduction at the Δ resonance that multipole analysis of data of comparable accuracy and completeness can be expected to determine the dominant electromagnetic multipole amplitudes with relatively little ambiguity due

to the tails of underlying nondominant resonances. Since the analyses of previous experiments demonstrated that η electroproduction for $W \approx 1.535$ GeV is also dominated by single resonance, we expect that multipole analysis of these proposed data will also be relatively insensitive to uncertainties in nondominant resonances. However, the response functions themselves will provide stringent tests of models with or without multipole analysis.

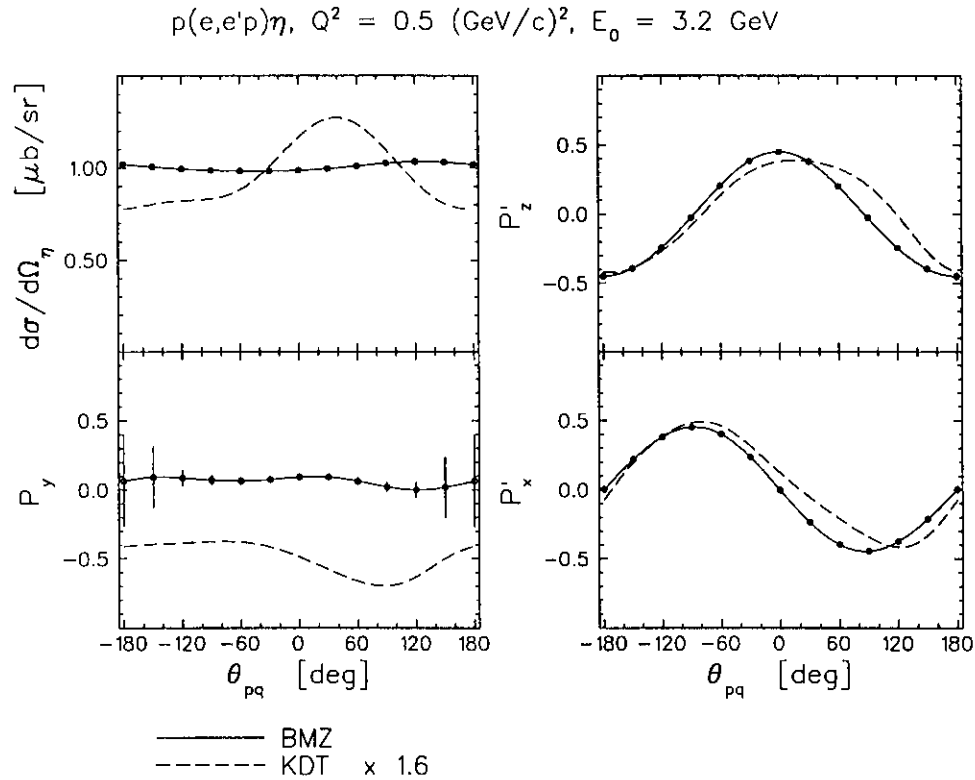


FIG. 16. Proposed measurements for $W = 1.535$ GeV and $Q^2 = 0.5 \text{ (GeV/c)}^2$ with projected statistical uncertainties. The solid lines are based upon the BMZ model and the dashed upon the KDT model scaled by a factor of 1.6.

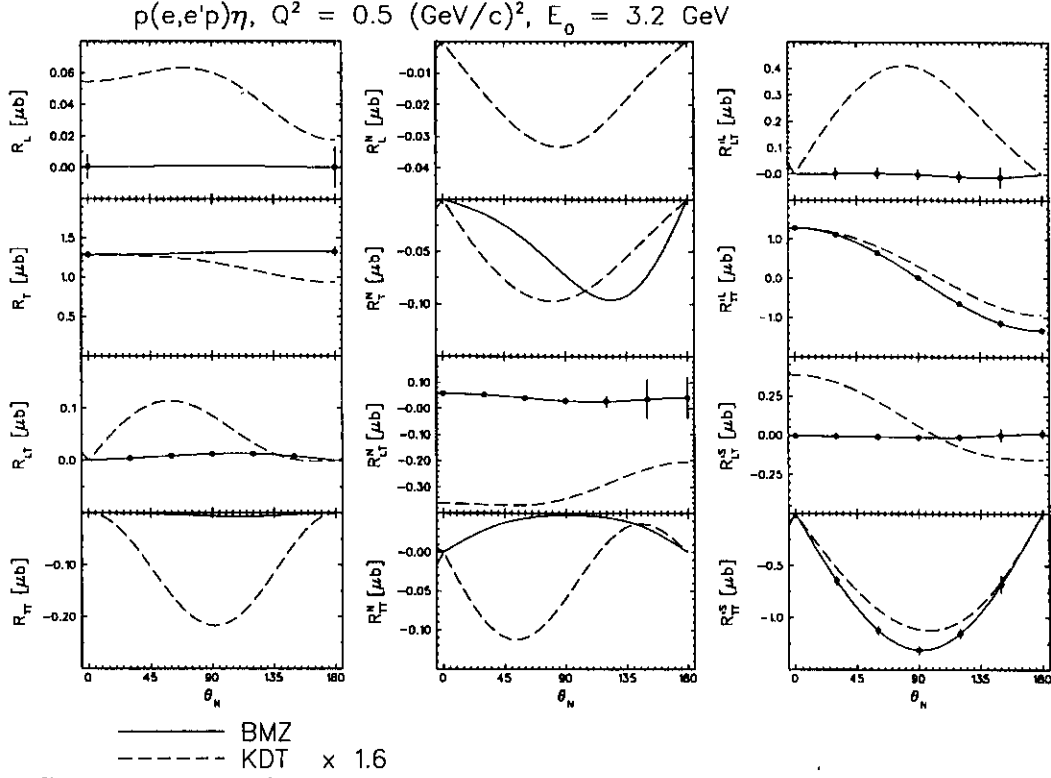


FIG. 17. Response functions with projected statistical uncertainties extracted from proposed measurements for $W = 1.535 \text{ GeV}$ and $Q^2 = 0.5 \text{ (GeV/c)}^2$. The solid lines are based upon the BMZ model and the dashed upon the KDT model scaled by a factor of 1.6.

IV. BEAM TIME REQUEST

Table VIII presents a summary of our beam time request. We estimate that approximately 36 hours will be needed for initial set up and tests, assuming that the operation of the target, spectrometers, and focal-plane polarimeter have already been established by first-generation experiments. We estimate that approximately two hours will be needed for each of the 11 angle and/or momentum changes. The production runs listed in Table VI require an estimated total of approximately 564 hours to achieve the desired statistical accuracy. Therefore, our request totals 624 hours.

TABLE VIII. Beam Time Request

initial setup and test	36
production runs	564
angle/momentum changes	24
total	624

APPENDIX A: OBSERVABLES AND RESPONSE FUNCTIONS

The kinematics for meson electroproduction are illustrated in Fig. 18. It is convenient to label the meson π and to interpret the label as referring to either a π , η , or other meson as the context requires. The angle between the leptonic scattering plane (containing the initial and final electron 3-vectors) and the hadronic reaction plane (containing the 3-momentum transfer \mathbf{q} and the final nucleon 3-momentum \mathbf{p}_{N_f}) is denoted by $\phi_N = \phi_\pi - 180^\circ$. The angles between the 3-momentum transfer and the laboratory momenta of the nucleon and the meson are denoted by θ_N and θ_π , respectively. Note that for $\phi_N = 0^\circ$ and $\theta_N > 0^\circ$, the nucleon recoils at a more forward angle than the 3-momentum transfer. The hadronic center of momentum frame is defined by the condition $\mathbf{q}^* + \mathbf{p}_{N_i}^* = \mathbf{p}_{N_f}^* + \mathbf{p}_\pi^* = \mathbf{0}$. The response functions can be considered functions of the invariant quantities

$$Q^2 = -q^2 = -(k_i - k_f)^2 = 2k_i k_f \sin^2(\theta_e/2)$$

$$W = \sqrt{s} = \sqrt{(q^* + p_{N_i}^*)^2} = \sqrt{(p_\pi^* + p_{N_f}^*)^2} = E_\pi^* + E_{N_f}^*$$

and the c. m. recoil nucleon angle $\theta_N^* = 180^\circ - \theta_\pi^*$.

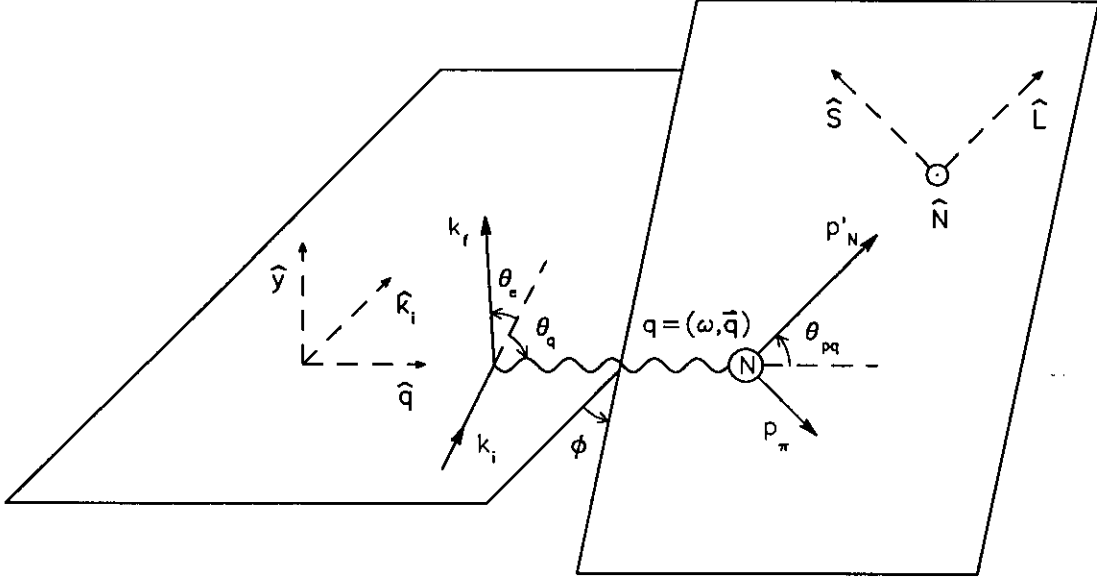


FIG. 18. Kinematics for meson production. k_i , k_f represent initial and final electron 4-vectors, q the 4-momentum transfer, p_π the meson and p_N the nucleon 4-momenta.

The differential cross section for coincident scattering of polarized electrons, here the $p(\vec{e}, e'\vec{p})\pi$ reaction, can be expressed as

$$\frac{d^5\sigma_{hs}}{d\epsilon_f d\Omega_e d\Omega_x} = \sigma_0 [1 + \mathbf{P} \cdot \boldsymbol{\sigma} + h(A + \mathbf{P}' \cdot \boldsymbol{\sigma})] \quad (\text{A1})$$

where σ_0 is the unpolarized differential cross section, A is the beam analyzing power, P is the induced or helicity-independent recoil polarization, P' is the polarization transfer or helicity-dependent recoil polarization, s indicates the nucleon spin projection upon σ , and h is the beam helicity. Thus, the net polarization of the recoil nucleon, Π has two contributions of the form

$$\Pi = P + hP' . \quad (\text{A2})$$

It is customary to express the differential cross section in terms of laboratory quantities for the electron and center-of-mass quantities for the hadrons, such that

$$\sigma_0 = K \tilde{\sigma}_0 = K^* \tilde{\sigma}_0 \frac{d\Omega_N^*}{d\Omega_N} \quad (\text{A3})$$

where

$$K^* = \frac{p^* W}{k_\gamma m_p} \Gamma_\gamma \quad (\text{A4})$$

is a phase-space factor,

$$\Gamma_\gamma = \frac{\alpha}{2\pi^2} \frac{k_f k_\gamma}{k_i Q^2} \frac{1}{1 - \epsilon} \quad (\text{A5})$$

is the virtual photon flux,

$$\epsilon = \left(1 + 2 \frac{|\mathbf{q}|^2}{Q^2} \tan^2 \frac{\theta_e}{2} \right)^{-1} \quad (\text{A6})$$

is the virtual photon transverse polarization, which is invariant with respect to colinear boosts, and

$$\epsilon_L = \frac{Q^2}{(\omega^*)^2} \epsilon \quad (\text{A7})$$

is the virtual photon longitudinal polarization in the cm frame. The quantity

$$k_\gamma = \frac{W^2 - m_p^2}{2m_p} \quad (\text{A8})$$

can be interpreted as the energy a real photon would need to excite the same transition.

The recoil polarization is usually calculated with respect to the helicity frame defined by the basis vectors

$$\hat{L} = \frac{\mathbf{P}_N^*}{|\mathbf{P}_N^*|} \quad (\text{A9a})$$

$$\hat{N} = \frac{\mathbf{q}^* \times \hat{L}}{|\mathbf{q}^* \times \hat{L}|} \quad (\text{A9b})$$

$$\hat{S} = \hat{N} \times \hat{L}. \quad (\text{A9c})$$

This basis is well defined when θ_N is not equal to 0° or 180° , but difficulties arise when \mathbf{q}^* and \mathbf{p}_N^* are either parallel or antiparallel and ϕ_N loses physical meaning. These cases are conventionally handled by first rotating the reaction plane to ϕ_N as it would be in non-parallel kinematics, and then taking the limit $\theta_N \rightarrow 0^\circ$ or $\theta_N \rightarrow 180^\circ$ as required. Note that since the basis vectors \hat{S} and \hat{N} reverse directions when $\phi \rightarrow \phi + \pi$, the corresponding components of the recoil polarizations also tend to reverse sign even when there is no physical asymmetry with respect to ϕ ; this behavior is simply an artifact of the basis.

Since the recoil polarization is measured in the laboratory frame, it is also useful to employ an alternative basis in which

$$\hat{z} = \frac{\mathbf{p}_N}{|\mathbf{p}_N|} \quad (\text{A10a})$$

$$\hat{y} = \frac{\mathbf{k}_i \times \mathbf{k}_f}{|\mathbf{k}_i \times \mathbf{k}_f|} \quad (\text{A10b})$$

$$\hat{x} = \hat{y} \times \hat{z} . \quad (\text{A10c})$$

Furthermore, the polarization vector must be transformed to the lab frame using a Wigner rotation [38]. Thus, when we express recoil polarization with respect to the $\{\hat{x}, \hat{y}, \hat{z}\}$ basis the transformation to the lab frame has been performed, whereas polarizations in the $\{\hat{S}, \hat{N}, \hat{L}\}$ basis remain in the cm frame. One advantage of presenting the recoil polarization in the lab or polarimeter basis, is that the recoil polarization components are continuous as \mathbf{p}_N moves through \mathbf{q} from one side to the other. Unlike \hat{S} and \hat{N} , \hat{x} and \hat{y} do not reverse directions when $\phi \rightarrow \phi + \pi$. For coplanar kinematics it then becomes convenient to use angles $-\pi \leq \theta_{pq} \leq \pi$ where for \hat{y} upwards $\theta_{pq} > 0$ refers to \mathbf{p}_N forward of \mathbf{q} .

The observables can be further decomposed into kinematical factors, ν_α , which depend only upon electron kinematics and response functions, R_α which carry the hadronic information. Regrettably, no accepted standard for the signs and normalizations of the response functions has gained wide acceptance. We have chosen a set of conventions in which all of the response functions enter the formulas with positive signs and all of the kinematical factors are also positive. We choose to express the azimuthal dependence in terms of ϕ_N because the nucleon is detected rather than the meson. Finally, we have evaluated the longitudinal polarization of the virtual photon in the c.m. frame. The observables are then related to response functions according to

$$\begin{aligned} \tilde{\sigma}_0 &= \nu_L R_L + \nu_T R_T + \nu_{LT} R_{LT} \cos \phi_N + \nu_{TT} R_{TT} \cos 2\phi_N \\ \tilde{\sigma}_0 A &= \nu'_{LT} R'_{LT} \sin \phi_N \\ \tilde{\sigma}_0 P_N &= [\nu_L R_L^N + \nu_T R_T^N + \nu_{LT} R_{LT}^N \cos \phi_N + \nu_{TT} R_{TT}^N \cos 2\phi_N] \\ \tilde{\sigma}_0 P_m &= [\nu_{LT} R_{LT}^m \sin \phi_N + \nu_{TT} R_{TT}^m \sin 2\phi_N] \quad (m = L, S) \\ \tilde{\sigma}_0 P'_N &= \nu'_{LT} R'_{LT} \sin \phi_N \\ \tilde{\sigma}_0 P'_m &= [\nu'_{LT} R'^m_{LT} \cos \phi_N + \nu'_{TT} R'^m_{TT}] \quad (m = L, S) \end{aligned}$$

where the kinematical factors

$$\begin{aligned}\nu_L &= \epsilon_L & \nu_T &= 1 \\ \nu_{LT} &= [2\epsilon_L(1 + \epsilon)]^{\frac{1}{2}} & \nu_{TT} &= \epsilon \\ \nu'_{LT} &= [2\epsilon_L(1 - \epsilon)]^{\frac{1}{2}} & \nu'_{TT} &= [1 - \epsilon^2]^{\frac{1}{2}}\end{aligned}$$

are expressed in terms of the polarization of the virtual photon.

It is also useful to define unpolarized partial cross sections such that

$$\frac{d\sigma}{d\Omega} = \frac{d\sigma_T}{d\Omega} + \epsilon \frac{d\sigma_L}{d\Omega} + [\epsilon(1 + \epsilon)]^{1/2} \frac{d\sigma_{LT}}{d\Omega} \cos \phi + \epsilon \frac{d\sigma_{TT}}{d\Omega} \cos 2\phi \quad (\text{A11})$$

where the kinematic factors are based on common conventions but are different from those we employed for the response functions. Finally, integrated longitudinal and transverse cross sections are defined as

$$\sigma_{tot} = \int d\Omega \frac{d\sigma_0}{d\Omega} = \sigma_T + \epsilon\sigma_L \quad (\text{A12a})$$

$$\sigma_L = \int d\Omega \frac{d\sigma_L}{d\Omega} \quad (\text{A12b})$$

$$\sigma_T = \int d\Omega \frac{d\sigma_T}{d\Omega} \quad (\text{A12c})$$

[Note that the definition of σ_L depends upon the conventions used for the kinematical factors.]

Considerable simplification of the spin structure of the reaction is obtained for parallel kinematics. Azimuthal symmetry around \mathbf{q} eliminates those response functions whose contributions to the observables depend upon the orientation of the reaction plane and also requires $R_{LT}^N = R_{LT}^S$ and $R_{LT}'^N = -R_{LT}'^S$. Hence, there remain at most five independent response functions in parallel kinematics. The expressions relating observables to response functions then reduce to

$$\tilde{\sigma}_0 = \nu_L R_L + \nu_T R_T \quad (\text{A13a})$$

$$\tilde{\sigma}_0 \Pi_N = \nu_{LT} R_{LT}^N \quad (\text{A13b})$$

$$\tilde{\sigma}_0 \Pi_S = h\nu'_{LT} R_{LT}'^S \quad (\text{A13c})$$

$$\tilde{\sigma}_0 \Pi_L = h\nu'_{TT} R_{TT}'^L. \quad (\text{A13d})$$

Thus, polarization measurements permit certain individual response functions to be isolated. Measurement of the induced polarization P_N for parallel kinematics yields R_{LT}^N at $\theta_{pq} = 0^\circ$ or 180° directly, whereas measurement of P'_S or P'_L yields $R_{LT}'^S$ or $R_{TT}'^L$, respectively.

TABLE IX. Properties of the Response Functions for the $A(\vec{e}, e'\vec{N})B$ Reaction. The constraints among response functions for parallel/antiparallel kinematics are indicated by the upper/lower choices of signs. The phase column indicates that a given response function is obtained either from the real part or the imaginary part of products of two amplitudes.

response function	helicity dependence	survives		phase	azimuthal dependence
		in plane	parallel		
R_L	X	✓	✓	Re	1
R_T	X	✓	✓	Re	1
R_{LT}	X	✓	X	Re	$\cos \phi$
R_{TT}	X	✓	X	Re	$\cos 2\phi$
R'_{LT}	✓	X	X	Im	$\sin \phi$
R_L^N	X	✓	X	Im	1
R_T^N	X	✓	X	Im	1
R_{LT}^N	X	✓	✓	Im	$\cos \phi$
R_{TT}^N	X	✓	X	Im	$\cos 2\phi$
R'^N_{LT}	✓	X	$\mp R'^S_{LT}$	Re	$\sin \phi$
R^L_{LT}	X	X	X	Im	$\sin \phi$
R'^L_{LT}	✓	✓	X	Re	$\cos \phi$
R^L_{TT}	X	X	X	Im	$\sin 2\phi$
R'^L_{TT}	✓	✓	✓	Re	1
R^S_{LT}	X	X	$\pm R^N_{LT}$	Im	$\sin \phi$
R'^S_{LT}	✓	✓	✓	Re	$\cos \phi$
R^S_{TT}	X	X	X	Im	$\sin 2\phi$
R'^S_{TT}	✓	✓	X	Re	1

**APPENDIX B: MULTIPOLE DECOMPOSITION ASSUMING S_{11}
DOMINANCE**

KDT [10] presented multipole decompositions for the complete set of response functions assuming dominance of the S_{11} amplitudes and including interferences with P_{11} and D_{13} contributions. Selected results are reproduced below:

$$\begin{aligned}
 R_T &= |E_{0+}|^2 - \text{Re} \left\{ E_{0+}^* \left[2 \cos \Theta M_{1-} - (3 \cos^2 \Theta - 1) (E_{2-} - 3M_{2-}) \right] \right\} \\
 R_L &= |L_{0+}|^2 + 2 \text{Re} \left\{ L_{0+}^* \left(\cos \Theta L_{1-} - 2 (1 - 3 \cos^2 \Theta) L_{2-} \right) \right\} \\
 R_{LT} &= -\sin \Theta \text{Re} \left\{ E_{0+}^* (L_{1-} + 6 \cos \Theta L_{2-}) + L_{0+}^* (M_{1-} + 3 \cos \Theta (M_{2-} - E_{2-})) \right\} \\
 R_{TT} &= -3 \sin^2 \Theta \text{Re} \left\{ E_{0+}^* (E_{2-} + M_{2-}) \right\} \\
 R_{LT}^N &= -\text{Im} \left\{ L_{0+}^* E_{0+} + E_{0+}^* \left(-\cos \Theta L_{1-} + 2 (1 - 3 \cos^2 \Theta) L_{2-} \right) \right. \\
 &\quad \left. + L_{0+}^* \left(-\cos \Theta M_{1-} + (3 \cos^2 \Theta - 2) E_{2-} - 3 \cos^2 \Theta M_{2-} \right) \right\} \\
 R_{LT}^S &= \text{Re} \left\{ \cos \Theta L_{0+}^* E_{0+} + E_{0+}^* (L_{1-} + 4 \cos \Theta L_{2-}) \right. \\
 &\quad \left. + L_{0+}^* (-M_{1-} + \cos \Theta (E_{2-} - 3M_{2-})) \right\} \\
 R_{LT}^L &= \sin \Theta \text{Re} \left\{ L_{0+}^* E_{0+} - 2 E_{0+}^* L_{2-} \right. \\
 &\quad \left. + L_{0+}^* (E_{2-} + 3M_{2-}) \right\} \\
 R_{TT}^S &= -\sin \Theta \left[|E_{0+}|^2 - \text{Re} \left\{ E_{0+}^* (E_{2-} - 3M_{2-}) \right\} \right] \\
 R_{TT}^L &= \cos \Theta |E_{0+}|^2 - 2 \text{Re} \left\{ E_{0+}^* [M_{1-} - \cos \Theta (E_{2-} - 3M_{2-})] \right\}
 \end{aligned}$$

Although these formulas are expressed in terms of meson angles and have not been translated according to our conventions, they nevertheless serve to delineate the important contributions to the separated response functions.

For our purposes it is important to recognize that the P_{11} resonances do not contribute in first-order to R_{TT}^S and that $\text{Re} E_{0+}^* M_{1-}$ can be identified from the isotropic part of R_{TT}^L . Furthermore, the D_{13} contributions to both R_{TT}^S and R_{TT}^L involve the same linear combination of E_{2-} and M_{2-} amplitudes but enter with opposite signs relative to $|E_{0+}|^2$. Therefore, although model calculations suggest that the D_{13} contribution to R_{TT}^S is negligible, it can in principle be isolated and subtracted by analyzing R_{TT}^L also.

APPENDIX C: SYMMETRIES FOR SUPERPARALLEL KINEMATICS

In this section we outline the derivation of the symmetry property $R_{TT}^L = \pm R_T$ for parallel (antiparallel) kinematics that applies to the $A(\vec{e}, e'\vec{N})B$ reaction when the spin of either A or B is $\frac{1}{2}$ and the other 0. Conditions in which the both the recoil momentum and the target or recoil polarization are parallel to \mathbf{q} are sometimes described as "superparallel" kinematics [39]. Some of the implications of this symmetry have been considered for nucleon knockout reactions upon spin-0 targets which leave the residual nucleus with spin- $\frac{1}{2}$ [40] and for electron scattering by a polarized spin- $\frac{1}{2}$ target [41]. Raskin and Donnelly [42] also mention this symmetry for pion electroproduction but do so in the context of a multipole expansion based upon $\Delta(1232)$ dominance, which is not really necessary. The complete tables of response functions expressed in terms of helicity amplitudes for pseudoscalar meson production which can be found in Refs. [10,43] implicitly contain the results below. The present derivation assumes that the reaction is mediated by one-photon exchange and conserves parity, but makes no other assumptions about the details of the transition amplitudes. In particular, it is not necessary to assume that a single resonance dominates.

The reaction amplitudes for any $A(e, e'N)B$ process where A has spin- $\frac{1}{2}$ and B spin-0 that is governed by one-photon exchange mechanism can be expressed in terms of helicity amplitudes of the form

$$H_{\lambda_f \lambda_i \lambda_\gamma}(Q^2, W, \theta_N^*, \phi_N) = \langle \lambda_f | \mathcal{F}_\mu \epsilon^\mu | \lambda_i, \lambda_\gamma \rangle \quad (\text{C1})$$

where λ_i and λ_f are the initial and final helicities of the nucleon, λ_γ is the helicity of the virtual photon, \mathcal{F}^μ is an appropriately normalized transition current operator, and ϵ^μ is the virtual-photon polarization. Since parity conservation requires

$$|H_{-\lambda_f - \lambda_i - \lambda_\gamma}| = |H_{\lambda_f \lambda_i \lambda_\gamma}|, \quad (\text{C2})$$

it is sufficient to consider the six independent amplitudes [44,45]

$$H_1 = \langle -\frac{1}{2} | \mathcal{F}_\mu \epsilon^\mu | -\frac{1}{2}, 1 \rangle \quad (\text{C3a})$$

$$H_2 = \langle -\frac{1}{2} | \mathcal{F}_\mu \epsilon^\mu | +\frac{1}{2}, 1 \rangle \quad (\text{C3b})$$

$$H_3 = \langle +\frac{1}{2} | \mathcal{F}_\mu \epsilon^\mu | -\frac{1}{2}, 1 \rangle \quad (\text{C3c})$$

$$H_4 = \langle +\frac{1}{2} | \mathcal{F}_\mu \epsilon^\mu | +\frac{1}{2}, 1 \rangle \quad (\text{C3d})$$

$$H_5 = \langle +\frac{1}{2} | \mathcal{F}_\mu \epsilon^\mu | +\frac{1}{2}, 0 \rangle \quad (\text{C3e})$$

$$H_6 = \langle +\frac{1}{2} | \mathcal{F}_\mu \epsilon^\mu | -\frac{1}{2}, 0 \rangle. \quad (\text{C3f})$$

Due to the absence of orbital angular momentum in the initial state or spin in the undetected recoil particle (B), the angular momentum projected onto the virtual photon direction reduces to $J_z = \lambda_\gamma - \lambda_i = \pm\lambda_f$ for parallel or antiparallel kinematics, where the upper sign applies to parallel and the lower to antiparallel kinematics. Hence, only H_4 and H_6 contribute to parallel or H_2 and H_5 to antiparallel kinematics.

With only two these helicity amplitudes surviving in parallel kinematics there can be only four independent response functions. Thus, evaluating the response functions for recoil polarization one finds

$$R_L \longrightarrow |H_6|^2 \quad (\text{C4a})$$

$$R_T \longrightarrow \frac{1}{2}|H_4|^2 \quad (\text{C4b})$$

$$R'_{TT} \longrightarrow \frac{1}{2}|H_4|^2 \quad (\text{C4c})$$

$$R'^S_{LT} \longrightarrow -\frac{1}{\sqrt{2}}\text{Re}H_4H_6^* \quad (\text{C4d})$$

$$R^N_{LT} \longrightarrow \frac{1}{\sqrt{2}}\text{Im}H_4H_6^* \quad (\text{C4e})$$

in parallel kinematics, or

$$R_L \longrightarrow |H_5|^2 \quad (\text{C5a})$$

$$R_T \longrightarrow \frac{1}{2}|H_2|^2 \quad (\text{C5b})$$

$$R'^L_{TT} \longrightarrow -\frac{1}{2}|H_2|^2 \quad (\text{C5c})$$

$$R'^S_{LT} \longrightarrow -\frac{1}{\sqrt{2}}\text{Re}H_2H_5^* \quad (\text{C5d})$$

$$R^N_{LT} \longrightarrow -\frac{1}{\sqrt{2}}\text{Im}H_2H_5^* \quad (\text{C5e})$$

in antiparallel kinematics; very similar results are also obtained for target polarization. Therefore, it is possible to obtain both the magnitudes and the relative phases of the H_4 and H_6 helicity amplitudes in parallel kinematics or the H_2 and H_5 amplitudes in antiparallel kinematics using either recoil or target polarization measurements.

It is also worth noting that H_2 and H_6 flip the nucleon helicity, whereas H_4 and H_5 do not. Furthermore, for parallel (antiparallel) kinematics helicity nonflip (flip) corresponds to spin flip. Hence, for superparallel kinematics R'^L_{TT} or R_T is driven by the spin-flip part of the transverse current.

These relationships can also be used to establish bounds upon the longitudinal component of the recoil polarization. Recognizing that

$$\Pi'_L = \frac{\pm \nu'_{TT} R_T}{\nu_T R_T + \nu_L R_L} = \frac{\pm \nu'_{TT}}{\nu_T + \nu_L \mathcal{R}_\pm} = \frac{\pm [1 - \epsilon^2]^{\frac{1}{2}}}{1 + \epsilon_L \mathcal{R}_\pm} \quad (\text{C6})$$

where

$$\mathcal{R}_\pm(Q^2, W) = \left. \frac{R_L(Q^2, W, \theta_N^*)}{R_T(Q^2, W, \theta_N^*)} \right|_{\theta_N^*=0, \pi} \quad (\text{C7})$$

is the ratio between the longitudinal and transverse response functions for parallel (antiparallel) kinematics, we find that for superparallel kinematics

$$|\Pi'_L| \leq \frac{\nu'_{TT}}{\nu_T} = [1 - \epsilon^2]^{\frac{1}{2}} \quad (\text{C8})$$

where ϵ is the polarization of the virtual photon. Thus, the ratio between the magnitudes of the relevant longitudinal and transverse helicity amplitudes can be obtained from the reduction of the longitudinal component of the recoil polarization for superparallel kinematics from the maximum value that could have been realized for a purely transverse spin-flip process.

Therefore, the symmetry property $R_{TT}^L = \pm R_T$, with upper (lower) sign for parallel (antiparallel) kinematics, applies to pseudoscalar meson production and is quite general, requiring only one-photon exchange and parity conservation. It is important to recognize that this symmetry does not depend upon dominance of any particular resonance and applies equally well to the resonant and nonresonant contributions. However, it need not apply to more complicated background processes such as $p(e, e'N)\pi\pi$. Fortunately, those contributions should vary slowly with missing mass and can be subtracted from the η production peak. Nor can this result be used to obtain the full angular distribution of R_T without Rosenbluth separation. Nevertheless, the ability to separate R_L and R_T in parallel and/or antiparallel kinematics using recoil polarization measurements without Rosenbluth separation can be very helpful in testing models and is a useful supplement to the traditional cross section method.

REFERENCES

- [1] R. W. Lourie, Nucl. Phys. **A509**, 653 (1990).
- [2] R. W. Lourie, Zeit. Phys. **C 50**, 345 (1991).
- [3] R. Haidan, Ph.D. thesis, Universität Hamburg, 1979.
- [4] F. W. Brasse *et al.*, Zeit. Phys. **C 22**, 33 (1984).
- [5] M. Warns, H. Schröder, W. Pfeil, and H. Rollnick, Zeit. Phys. **C 45**, 613 (1990).
- [6] M. Warns, H. Schröder, W. Pfeil, and H. Rollnick, Zeit. Phys. **C 45**, 627 (1990).
- [7] W. Konen and H. J. Weber, Phys. Rev. **D 41**, 2201 (1990).
- [8] R. H. Stanley and H. J. Weber, Phys. Rev. **C 52**, 435 (1995).
- [9] L. A. Copley, G. Karl, and E. Obryk, Nucl. Phys. **B13**, 303 (1969).
- [10] G. Knöchlein, D. Drechsel, and L. Tiator, Zeit. Phys. **A 352**, 327 (1995).
- [11] S. Capstick and B. D. Keister, Phys. Rev. **D 51**, 3598 (1995).
- [12] B. Krusche *et al.*, Phys. Rev. Lett. **74**, 3736 (1995).
- [13] C. A. Heusch, C. Y. Prescott, L. S. Rochester, and B. D. Winstein, Phys. Rev. Lett. **19**, 1381 (1970).
- [14] J. W. Price *et al.*, Phys. Rev. **C 51**, R2283 (1995).
- [15] S. A. Dytman *et al.*, Phys. Rev. **C 51**, 2710 (1995).
- [16] S. Homma *et al.*, J. Phys. Soc. Japan **57**, 828 (1988).
- [17] F. W. Brasse *et al.*, Nucl. Phys. **B139**, 37 (1978).
- [18] H. Breuker *et al.*, Phys. Lett. **74B**, 409 (1978).
- [19] J.-C. Alder *et al.*, Nucl. Phys. **B91**, 386 (1975).
- [20] U. Beck *et al.*, Phys. Lett. **51B**, 103 (1974).
- [21] P. S. Kummer *et al.*, Phys. Rev. Lett. **30**, 873 (1973).
- [22] B. G. Ritchie, CEBAF proposal E-91-008.
- [23] S. Dytman and K. Giovanetti, CEBAF proposal E-89-039.
- [24] L. Tiator, C. Bennhold, and S. S. Kamalov, Nucl. Phys. **A580**, 455 (1994).
- [25] M. Benmerrouche, N. C. Mukhopadhyay, and J. F. Zhang, Phys. Rev. **D 51**, 3237 (1995).
- [26] T. M. Payerle and J. J. Kelly, User Manual for *EPIP*ROD, 1996.
- [27] Particle Data Group, Rev. Mod. Phys. **48**, II, S1 (1976).
- [28] G. E. Brown, M. Rho, and W. Weise, Nucl. Phys. **A454**, 669 (1986).
- [29] C. Bennhold and H. Tanabe, Nucl. Phys. **A530**, 625 (1991).
- [30] M. Benmerrouche, N. C. Mukhopadhyay, and J. F. Zhang, Phys. Rev. Lett. **77**, 4716 (1996).
- [31] R. Koniuck and N. Isgur, Phys. Rev. **D 21**, 1868 (1980).
- [32] M. Benmerrouche, Ph.D. thesis, Rensselaer Polytechnic Institute, 1992.
- [33] J. I. McIntyre, Ph.D. thesis, College of William and Mary, 1996.
- [34] K. Gustafsson, Cryotarget density dependence on beam current, Hall C report, 1996.
- [35] A. Sarty, Monte Carlo code for η production, 1996.
- [36] J. W. Lightbody, Jr. and J. S. O'Connell, Computers in Physics **2**, 57 (1988).
- [37] R. W. Lourie *et al.*, CEBAF proposal PR 91-011: Investigation of the $N \rightarrow \Delta$ Transition via Polarization Observables in Hall A.

- [38] V. Dmitrasinovi, Phys. Rev. C **47**, 2195 (1993).
- [39] S. Boffi, C. Giusti, and F. D. Pacati, Phys. Rep. **226**, 1 (1993).
- [40] S. Boffi, C. Giusti, and F. D. Pacati, Nucl. Phys. A**476**, 617 (1988).
- [41] C. Giusti and F. D. Pacati, Nucl. Phys. A**504**, 685 (1989).
- [42] A. S. Raskin and T. W. Donnelly, Ann. Phys. (N.Y.) **191**, 78 (1989).
- [43] D. Drechsel and L. Tiator, J. Phys. G **18**, 449 (1992).
- [44] H. F. Jones, Il Nuovo Cimento **40**, 1018 (1965).
- [45] R. L. Walker, Phys. Rev. **182**, 1729 (1969).